Effect of topographic slope on the export of nitrate in humid catchments: a 3D model study

Jie Yang[1], Qiaoyu Wang[1], Ingo Heidbüchel[2, 4], Chunhui Lu[1], Yueqing Xie[3], Andreas Musolff[2], and Jan H. Fleckenstein[2, 4]

[1]State Key Laboratory of Hydrology-Water Resources and Hydraulic Engineering, Hohai University, Nanjing, China
[2]UFZ - Helmholtz-Centre for Environmental Research GmbH, Department of Hydrogeology, Leipzig, Germany
[3]School of Earth Sciences and Engineering, University of Nanjing, Nanjing, China
[4]Hydrologic Modeling Unit, Bayreuth Center of Ecology and Environmental Research (BayCEER), University of Bayreuth, Bayreuth, Germany

Correspondence to: ~~Jie Yang (yangj@hhu.edu.cn);~~ Chunhui Lu (clu@hhu.edu.cn)

Key Points

- Young water fractions of Q and ET are correlated to topographic slope negatively and positively, respectively

- Flatter landscapes tend to retain more nitrogen mass in the soil and export less nitrogen mass to the stream

- A large young streamflow fraction is not sufficient for high in-stream nitrate concentrations.

Abstract. Excess export of nitrate to streams affects ecosystem structure and functions and has been an environmental issue attracting world-wide attention. The dynamics of catchment-scale solute export from diffuse nitrogen sources can be explained by the changes of dominant flow paths, as solute attenuation (including the degradation of nitrate) is linked to the age composition of outflow. Previous data driven studies suggested that catchment topographic slope has strong impacts on the age composition of streamflow and consequently on in-stream solute concentrations. However, the impacts have not been systematically assessed in terms of solute mass fluxes and solute concentration levels, particularly in humid catchments with strong seasonality in meteorological forcing. To fill this gap, we modeled the groundwater flow and nitrate transport for a small agricultural catchment in Central Germany. We used the fully coupled surface and subsurface numerical simulator HydroGeoSphere (HGS) to model groundwater and overland flow as well as nitrate transport. We computed the water ages using numerical tracer experiments. To represent various topographic slopes, we additionally simulated ten synthetic catchments generated by modifying the topographic slope from the real-world scenario. Results suggest a negative correlation between the young streamflow fraction and the topographic slope. This correlation is more pronounced in flat landscapes with slopes < 1:60. Flatter landscapes tend to retain more N mass in the soil (including mass degraded in soil) and export less N mass to the stream, due to reduced leaching and increased degradation. The mean in-stream nitrate concentration shows a decreasing trend in response to

35   a decreasing topographic slope, suggesting that a large young streamflow fraction is not sufficient for high in-stream

36   concentrations. Our results improve the understanding of nitrate export in response to topographic slope in a temperate

37   humid climate, with important implications for the management of stream water quality.

38

39   **Keywords**: topographic slope, coupled surface-subsurface model, young streamflow, in-stream nitrate,

40   HydroGeoSphere

41

1 Introduction

43   Globally nearly 40% of land is used for agricultural activities [*Foley et al.,* 2005], which constitutes the major source

44   of pollution with nutrients such as nitrate (referred as to $N-NO_3$ in this study). Excess export of nitrate to streams

45   threatens ecosystem structure and functions, as well as human health via drinking water [*Vitousek et al.,* 2009; *Alvarez-*

46   *Cobelas et al.,* 2008; *Dupas et al.*, 2017]. This has been an environmental issue attracting attention in Germany and

47   world-wide. The dynamics of nitrate export from diffuse nitrogen (N) sources are regulated by the dominant flow

48   paths that determine the speed at which precipitation travels through catchments before it reaches the stream [*Jasechko*

49   et al. 2016]. The process is subject to both hydrological and biogeochemical influences mediated by various factors

50   (e.g. catchment topography, aquifer properties, redox boundaries). From the perspective of sustainable intensification,

51   process understanding and assessment of potential effects of catchment topography on nitrate export are critical for

52   the management of water quality in connection with agricultural activity.

53   Field observations in central German catchments indicate that in-stream nitrate concentrations (C_Q) show significant

54   differences in mean concentrations and seasonal variations between downstream areas with gentle topography and

55   more mountainous upstream areas [*Dupas et al.*, 2017; *Nguyen et al.,* 2022]. This provides strong evidence that

56   catchment topographic slope can influence the nitrate export. In terms of water age analyses, *Jasechko* et al. [2016]

57   using oxygen isotope data from 254 watersheds worldwide showed significant negative correlation between the young

58   (age < 3 months) streamflow fraction and the mean topographic gradient. They stated that young streamflow is more

59   prevalent in flatter catchments as these catchments are characterized by shallow lateral flow, while it is less prevalent

60   in steeper mountainous catchments as these catchments promote deep vertical infiltration. This statistically significant

61   trend is consistent with the common finding that fast shallow flow paths produce young discharge and potentially

62   influence the in-stream solute concentrations [*Böhlke* et al. 2007; *Benettin* et al. 2015; *Hrachowitz* et al. 2016; *Blaen*

63   *et al.* 2017]. However, apart from these data-driven analyses, a more mechanistic examination/explanation with the

64   aid of fully resolved flow paths is still required. Wilusz et al. [2017] used a coupled rainfall-runoff and transit time

65   model to investigate the young streamflow fraction, with a focus on the effect of rainfall variability rather than on

66   topography and solute export. Zarlenga et al. [2022] numerically quantified the relative contributions of hillslopes and

67   the drainage network to age dynamics in streamflow, considering the influences of transmissivity and recharge,

68   without focusing on topographic slope. The effect of topographic slope on C_Q has rarely been subject to systematical

69   testing.

70 Seasonal fluctuation of C_Q is commonplace in catchments under seasonal hydrodynamic forcing. Field observations

71 in mountainous central German catchments indicate that nitrate concentrations, as well as the mass load, in streams

72 vary seasonally, with maxima during the wet winter and minima during the dry summer [*Dupas et al.*, 2017]. Data-

73 driven analyses by *Musolff et al.* [2015] and *Dupas et al.* [2017] suggested the systematic seasonal (de)activation of

74 N source zones as an explanation for such seasonal variability. Under wetter winter conditions the near-surface N

75 source zones in agricultural soils are connected to the stream by fast shallow flow paths. Under drier summer

76 conditions those N source zones are deactivated because their direct hydrologic connectivity to the stream is replaced

77 with deeper flow paths [*Dupas et al.*, 2017]. Based on high-frequency monitoring in the Wood Brook catchment in

78 the UK, *Blaen et al.* [2017] also reported mobilization of nitrate from the uppermost soil layers during high flow

79 conditions via shallow preferential flow paths, which would not occur during base flow in drier periods. This behavior

80 leads to a seasonally-variable nitrate loading due to changing flow paths and the associated variation in transit time

81 that has been observed in many catchments [*Benettin et al.*, 2015; *Hrachowitz et al.*, 2016; *Kaandorp et al.,* 2018;

82 *Rodriguez et al.*, 2018; *Yang et al.* 2018]. However, how this fluctuation behaves in response to catchment land surface

83 topography has not been assessed systematically yet. Such an assessment could improve our understanding of nitrate

84 export from catchments of different topographic slopes not only in terms of the mean concentration but also regarding

85 its temporal variation patterns.

86 Given that most of the above studies used data driven analysis, numerical modeling is an effective tool for the analysis

87 of water flow, age and solute transport, eliminating the need for large amounts of field data. ~~For example, *van der*~~

88 ~~*Velde et al.* [2012] constructed a lumped numerical nitrate transport model for the Hupsel Brook catchment in the~~

89 ~~Netherlands, without resolving the spatially-explicit details.~~ *Zarlenga and Fiori* [2020] presented a physically-based

90 framework to model transient water ages at the hillslope scale, which was later used to investigate the different impacts

91 of hillslopes and the channel network on water ages in catchments [*Zarlenga et al.*, 2022]. A number studies focused

92 on numerically simulating the nitrogen fluxes (or loads) in soil and groundwater [*Smith et al.,* 2004; *Rivett et al.,* 2008;

93 *Lindström et al.,* 2010*; van der Velde et al.,* 2012; *Van Meter et al.,* 2017; *X. Yang et al.,* 2018, 2019; *Kolbe et al.,*

94 2019; *Knoll et al.,* 2020; *Nguyen et al.,* 2021, 2022]. For example, *van der Velde et al.* [2012] constructed a lumped

95 numerical nitrate transport model for the Hupsel Brook catchment in the Netherlands~~, without resolving the spatially~~

96 ~~explicit details~~. *Lindström et al.* [2010] developed HYPE water quality model allowing for simulating the nitrogen

97 fluxes in soil. *Van Meter et al.* [2017] investigated the two-centuries nitrogen dynamics in the Mississippi and

98 Susquehanna River Basins using a TTD (transient time distribution) based transport approach. *X. Yang et al.* [2018]

99 developed the coupled mHM-Nitrate model, which can provide valuable insights int the spatial variability of water

100 and nitrate fluxes in catchment scale. *Nguyen et al.* [2021] further updated that model to the mHM-SAS model by

101 implementing the SAS-function based solute transport module [*Harman*, 2015, 2019; *Rinaldo et al.*, 2015; *van der*

102 *Velde et al*l., 2012], allowing for simulating the nitrate export from a Mesoscale Catchment. However, most of these

103 works provided little information on the spatially-explicit details (such as the flow field) for interpreting the nitrate

104 dynamics. Physically-based hydrogeological models (like, e.g., HydroGeoSphere [*Therrien* et al., 2010]) resolve the

105 spatially-explicit details within a catchment including the full variability of 3D flow paths in the subsurface, helping

106 to understand the seasonally changing flow patterns in response to different catchment topographies. Additionally, the

107   widely used fully-coupled surface-subsurface technology simulates the catchment as an integrated system, providing

108   details of surface water-groundwater exchanges fluxes. These details help to identify paths of rapid discharge to the

109   land surface that can considerably improve the interpretation of nitrate-export patterns.

110   Transit time distributions (TTDs) have been widely used to interpret hydrological and chemical responses in catchment

111   outfluxes – both in discharge (Q) and in evapotranspiration (ET) [*Botter et al.*, 2010, 2011; *van der Velde et al.*, 2012;

112   *Heidbüchel et al.*, 2012; *Rinaldo et al.* 2015; *Harman et al.*, 2015; 2019]. They characterize how a catchment stores,

113   mixes and releases water as well as dissolved solutes at large spatial and temporal scales [*Benettin et al.*, 2015; *Harman*,

114   2015; *van der Velde et al.*, 2010, 2012; *Hrachowitz et al.*, 2015; *Van Meter et al.*, 2017]. Given that the nitrate

115   attenuation is linked to the age composition of outflow, the TTDs are ideal tools for interpreting the concentration

116   dynamics with regard to catchment topographic slope. Estimating water ages in natural catchments is still a challenge

117   due to varying climate conditions, as well as the errors in algorithms (e.g. errors in the flow field during particle

118   tracking) and limited computational capacity. *Yang et al*. [2018] used particle tracking to compute the age distributions

119   in the subsurface of a study catchment (while omitting the 4% of total discharge produced by direct surface runoff and

120   ignoring the frequent exchange fluxes that may be important for solute export due to their short transit times). Zarlenga

121   *et al*., [2022] used a physically-based semi-analytical model to compute the transient water ages in a catchment,

122   however, without considering surface runoff and hydrological losses (e.g. ET). In this study we determined the age

123   compositions of Q and ET using numerical tracer experiments, where advective-dispersive transport of the tracers was

124   solved using the fully-coupled surface-subsurface framework of HydroGeoSphere. The computed age dynamics based

125   on the tracer concentrations were representative as the tracers were able to track all the flow processes such as surface

126   runoff, groundwater flow and surface-subsurface interaction.

127   In this study, we attempted to systematically assess the effect of catchment topographic slope on the nitrate export

128   dynamics in terms of mass fluxes, concentration levels and its seasonal variability. We also seek mechanical

129   explanations for the previously found behaviors from data-driven studies (like, e.g., *Jasechko et al*. [2016]) with the

130   help of fully resolved flow paths. First, we selected a real-world small agricultural catchment 'Schäfertal' in Central

131   Germany, which is characterized by strong seasonality in hydrodynamic forcing with associated shifts in the dominant

132   flow paths [*Yang et al.*, 2018]. This catchment is typical for many catchments with hilly topography under a temperate

133   humid climate. We created eleven model scenarios by adjusting the mean slope of the real-world catchment while

134   preserving the aquifer heterogeneity. Next, we modeled the water flow and nitrate transport for each catchment. The

135   flow and transport were solved using the fully coupled surface and subsurface numerical simulator HydroGeoSphere,

136   and the water ages were computed using numerical tracer experiments. Finally, the modeled flowpaths, water ages, N

137   mass fluxes and nitrate concentrations under various topographic slopes were analyzed. Through this study, we aimed

138   to (1) examine the relationship between topographic slope and N mass fluxes, and to (2) assess C_Q and its seasonal

139   variation in response to different topographic slopes.

140

2 Data collection

2.1 Real-world and synthetic catchments

Our study was conducted on the catchment 'Schäfertal', situated in the lower part of the Harz Mountains, Central Germany (Figure 1a). The catchment has an area of 1.44 km^2. The hillslopes are mostly used for intensive agriculture while the valley bottom contains riparian zones with pasture and a small stream draining the water out of the catchment. The gauging station at the outlet of the catchment provides Q records. This gauging station is the only outlet for discharging water from the catchment, because a subsurface wall was erected underneath the gauging station across the valley to block subsurface flow out of the catchment. A meteorological station 200 m from the catchment outlet provides records of precipitation (J), air and soil temperatures, radiation and wind speed. The modeled catchment has a mean topographic slope of ~1:20, estimated using a cross-section perpendicular to the stream (Figure 1a). The aquifer thickness varies from ~5 m near the valley bottom to ~2 m at the top of the hillslope. Groundwater storage is low (~500 mm) in such a thin aquifer and mostly limited to the vicinity of the channel with the upper part of the hillslopes generally unsaturated. The stream bed has a depth of 1.5 m below the land surface. Aquifer properties (e.g. hydraulic conductivity) change from the hillslope, dominated by Luvisols and Cambisols, to the valley bottom, dominated by Gleysols and Luvisols [*Anis and Rode*, 2015]. Apart from that, the aquifer generally consists of two layers: the top layer of approximately 0.5 m thickness with higher porosity and a developed root zone from crops, and the base layer with smaller porosity due to high loam content [*Yang et al.*, 2018]. Subsequently, ten property zones were used (Figure 1b), with zonal parameter values following the model in *Yang et al.*, [2018] listed in Table 1.

Based on this real-world catchment, ten synthetic catchments were generated by adjusting elevations (land surface and aquifer bottom), such that the mean topographic slope ranges from 1:20 (steep) to 1:22, 1:25, 1:30, 1:40, 1:60, 1:80, 1:100, 1:200, 1:500 and 1:1000 (flat, Figure 1b). The aquifer depth and heterogeneity were preserved during the adjustments. In total, eleven catchments were used for flow and transport simulations. The catchment with the original topography (1:20) is selected as the base scenario.

2.2 Climate

The considered climate for the catchments was derived from the catchment 'Schäfertal' located in a region with temperate humid climate and pronounced seasonality. According to the meteorological data records from 1997 to 2007, the mean annual J and Q (per unit area) are 610 mm and 160 mm, respectively. Actual mean annual ET based on the ten-year water balance ($J = ET + Q$) is 450 mm. Mean annual potential ET is 630 mm [*Yang et al.*, 2018]. The humid climate is representative for wet regions, quantified by an aridity index (J / potential ET [*Li et al.,* 2019]) of 1.0. The ET is the main driver of the hydrologic seasonality as the precipitation is more uniformly distributed across the year (Figure 1c).
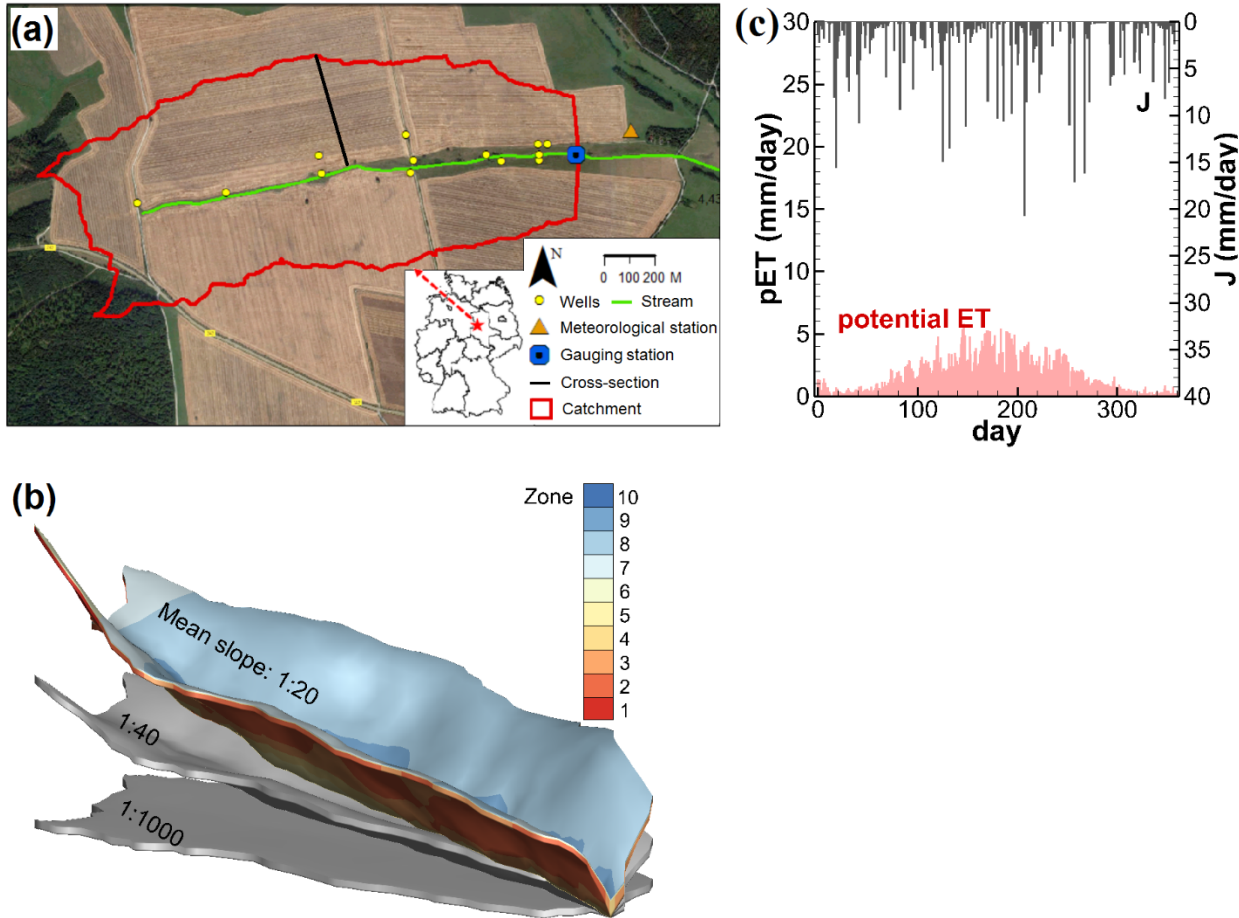
Figure 1.- (a) The catchment 'Schäfertal', Central Germany (background image from © Google Maps). (b) The catchments with mean topographic slopes of 1:20, 1:40 and 1:1000. (c) The measured precipitation J and the estimated potential evapotranspiration ET for the year 2005 under the ~~the~~ humid climate [*Yang et al.*, 2018]. Ten aquifer property zones in (b) were defined in the subsurface of the catchment for zonal parameter values (e.g. hydraulic conductivity).

3 Methods

3.1 Flow and nitrate transport

Flow model

It is necessary to solve both groundwater and surface water flow because the spatially-explicit details in the catchment including the specific flow paths and exchange fluxes are necessary to interpret the effect of varying topographic slope on nitrate transport. We simulated the flow system using the fully coupled surface and subsurface numerical model HydroGeoSphere, which solves for variably saturated groundwater flow with the Richards' equation and for surface flow with the diffusion-wave approximation of the Saint-Venant equations [*Therrien* et al., 2010]. Additionally, the exchange flux between groundwater and surface water can be implicitly simulated. The nitrate transport is simulated

190 in the groundwater flow, surface flow and exchanges fluxes by solving the advection-dispersion-diffusion equation

191 describing the conservation of nitrate mass. HydroGeoSphere has been successfully used to simulate catchment

192 hydrological processes and solute transport in many studies [e.g. *Therrien et al.*, 2010; *Yang et al.*, 2018], therefore

193 governing equations and technical details are not explicitly repeated here.

194 In our previous work *Yang et al.* [2018], a hydrological flow model has already been established for the catchment

195 'Schäfertal'. It was calibrated against measured groundwater levels and stream discharge Q. The optimized parameter

196 values are listed in Table 1. In this work, we performed our simulations based on that flow model, with the nitrate

197 transport process being added while maintaining the model setup. We provide a brief review of that flow model here.

198 Readers may refer to *Yang et al.* [2018] for a full description of the model and its calibration.

199 The modeled subsurface of the catchments was discretized into 9 horizontal layers between the land surface and the

200 aquifer base, with thinner layers in the upper part (0.1 m) to better represent the unsaturated zone and compute the ET.

201 In total, the subsurface was discretized by a mesh of 13860 prisms, with the horizontal size of the prisms ranging from

202 30 to 50 m. The topmost 1540 triangles were used to discretize the surface domain, where surface flow was simulated.

203 Ten property zones for the subsurface were defined (Figure 1b), being assigned with the zonal hydraulic conductivity

204 and porosity values (Table 1). ET was simulated as a combination of plant transpiration from the root zone (top 0.5 m

205 soil) and evaporation down to the evaporation depth (0.5 m), which are both constrained by soil water saturation.

206 Regarding the flow boundary conditions, spatially uniform and temporally variable J was applied to the land surface.

207 Spatially constant and temporally variable potential ET was applied to the aquifer top to calculate the actual ET. The

208 bottom of the aquifer was considered an impermeable boundary. A critical depth boundary condition was assigned to

209 the catchment outlet to simulate the stream discharge Q, which was compared to the measured Q during the calibration.

210 The software PEST [Doherty and Hunt, 2010] was used for the transient calibration. After calibration, the time-

211 variable groundwater levels were well replicated by the flow model for most of the wells, with mean coefficients of

212 determination (R^2) of 0.43. The fit between the simulated and measured Q was satisfactory with a R^2 of 0.61. The

213 calibrated model successfully simulated the flow system from 1997 to 2007.

214 In this study, we continued to use the above-described model setup, including the mesh, the parameters and the flow

215 boundary conditions, for the eleven catchments with different topography. Note that the mesh was adapted to the

216 change of the topography by changing node elevations vertically. However, to simplify the flow simulation and the

217 age computation (described in section 3.2), we selected the year 2005 as a representative year and assumed that all the

218 years have the identical climate (J and potential ET) as the year 2005. Therefore, J and potential ET of 2005 (Figure

219 1c) were cycled and applied to the catchments for all the simulated years.

220

221   **Table 1**. The key flow parameters and their values following *Yang et al*., [2018].

Parameter	Process	Type	Value
Hydraulic conductivity	Subsurface	zonal	Zonal values (refer to Yang et al., [2018])
Porosity	Subsurface	zonal	Zonal values (refer to Yang et al., [2018])
Residual saturation	Subsurface	uniform	0.08 [-]
Inverse of air entry pressure α	Subsurface	uniform	3.6 m^{-1}
Pore-size distribution index β	Subsurface	uniform	2 [-]
Manning roughness coefficient	Surface	uniform	$6.34 \cdot 10^{-6} \text{ day m}^{-1/3}$
Longitudinal dispersivity	Transport	uniform	8 m
Lateral and vertical dispersivity	Transport	uniform	0.8 m
Molecular diffusion coefficient	Transport	uniform	$10^{-9} \text{ m}^2 \text{ s}^{-1}$
Degradation coefficient	Transport	uniform	0.009 day^{-1}
Transpiration fitting parameters:			
C1	ET	uniform	0.17 [-]
C2	ET	uniform	0.00 [-]
C3	ET	uniform	3.00 [-]
Transpiration limiting saturations:			
Wilting point	ET	uniform	0.1 [-]
Field capacity	ET	uniform	0.2 [-]
Oxic limit	ET	uniform	0.9 [-]
Anoxic limit	ET	uniform	1.0 [-]
Evaporation limiting saturations:			
Minimum	ET	uniform	0.1 [-]
Maximum	ET	uniform	0.2 [-]

222

Parameter	Process	Type	Value
Hydraulic conductivity	Subsurface	zonal	Zonal values (range [$3.6 \cdot 10^{-5}$ - 2.0] m day^{-1})
Porosity	Subsurface	zonal	Zonal values (range [0.01 - 0.35])
Residual saturation	Subsurface	uniform	0.08 [-]
Inverse of air entry pressure α	Subsurface	uniform	3.6 m^{-1}
Pore-size distribution index β	Subsurface	uniform	2 [-]
Manning roughness coefficient	Surface	uniform	$6.34 \cdot 10^{-6}$ day m$^{-1/3}$
Longitudinal dispersivity	Transport	uniform	8 m
Lateral and vertical dispersivity	Transport	uniform	0.8 m
Molecular diffusion coefficient	Transport	uniform	10^{-9} m^2 s^{-1}
Degradation coefficient	Transport	uniform	0.009 day^{-1}
Transpiration fitting parameters:			
C1	ET	uniform	0.17 [-]
C2	ET	uniform	0.00 [-]
C3	ET	uniform	3.00 [-]
Transpiration limiting saturations:			
Wilting point	ET	uniform	0.1 [-]
Field capacity	ET	uniform	0.2 [-]
Oxic limit	ET	uniform	0.9 [-]
Anoxic limit	ET	uniform	1.0 [-]
Evaporation limiting saturations:			
Minimum	ET	uniform	0.1 [-]
Maximum	ET	uniform	0.2 [-]

223

224

225

Transport boundary conditions and parameters

226

227 The nitrogen (N) pool is formed in the soil zone of the catchments, representing a nitrate source zone. The N pool is

228 controlled by various complex processes. It is replenished by external inputs from atmospheric deposition, biological

229 fixation, animal manure from the pasture area, and fertilizer from the farmland on the hillslopes. Nitrate that can be

230 transported with water is formed and leached from this N pool by a microbiological immobile-mobile exchange

231 process [*Musolff* et al., 2017; *Van Meter* et al., 2017]. In our study, we employed the simplified framework by *Yang*

232 *et al.*, [2021] to track the fate of N in the N pool (Figure 2a). This framework was derived from the ELEMeNT

233 approach (Exploration of Long-tErM Nutrient Trajectories, Van Meter et al., 2017), which uses a parsimonious

234 modeling framework to estimate the biogeochemical legacy nitrate loading in the N pool and the N fluxes leaching

235 from the N pool to the groundwater. This framework assumes that total N load in the N pool is comprised by inorganic

236 N (SIN) and organic N (SON). Two types of SON are distinguished: active organic N (SON$_a$) with faster reaction

237 kinetics and protected organic N (SON$_p$) with slower reaction kinetics. It is assumed that the external N input

238 contributes only to the SON. The SON is mineralized into SIN. The SIN is further consumed by plant uptake and

239 denitrification, and finally leaches to groundwater as dissolved inorganic N (DIN, representing mainly nitrate in the

240 studied catchment [*Yang et al.*, 2018; *Nguyen et al.*, 2021]). The framework is acceptable due to the fact that most of

241 the nitrate fluxes from source zones has undergone biogeochemical transformation in the organic N pool [*Haag and*

242 *Kaupenjohann,* 2001]. The framework simplifies complexities of different N pools and transformations via

243 mineralization, dissolution, and denitrification within the soil zone [Lindström et al., 2010], while preserving the main

244 pathway for nitrate leachate.

245 The governing equations to calculate these N fluxes follow the ones in *Yang et al.*, [2021]. A specific portion (*h*) of

246 the external N input contributes to the SON_p pool, and the rest contributes to the SON_a pool. The portion *h* is the land-

247 use dependent protection coefficient [*Van Meter et al.*, 2017]. The mineralization and denitrification are described as

248 first order processes with rate coefficients k_a, k_p, and λ_s respectively, using:

$$MINE_a = k_a \cdot f(temp) \cdot SON_a \tag{1}$$

$$MINE_p = k_p \cdot f(temp) \cdot SON_p \tag{2}$$

$$DENI_s = \lambda_s \cdot SIN \tag{3}$$

252 where $MINE_a$, $MINE_p$, $DENI_s$ (kg ha^{-1} day^{-1}) are the mineralization rates for SON_a and SON_p, and denitrification rate

253 for SIN. k_a, k_p, and λ_s (day^{-1}) are coefficients for the first order processes. $f(temp)$ is a factor representing a constraint

254 by soil temperature [*Lindström et al.*, 2010]. Note that the mineralization and plant uptake occur in the N pool.

255 Denitrification can occur in both the N pool and later in groundwater. The plant uptake rate UPT follows the equation

256 used in the HYPE model [*Lindström* et al., 2010]:

$$UPT = \min (UPT_P, 0.8 \cdot SIN) \tag{4}$$

$$UPT_P = p1/p3 \cdot (\tfrac{p1-p2}{p2}) \cdot e^{-(DNO-p4)/p3} \Big/ (1 + (\tfrac{p1-p2}{p2}) \cdot e^{-(DNO-p4)/p3})^2 \tag{5}$$

259 where UPT and UPT_P (kg day^{-1} ha^{-1}) are the actual and potential uptake rates. The computation of UPT_P considers a

260 logistic plant growth function. *DNO* is the day number. *p1, p2, p3* are three parameters depending on the crop/plant

261 type, they are in the units of (kg ha^{-1}), (kg ha^{-1}), and (day), respectively. *p4* is the day number of the sowing date. The

262 leaching process allows for SIN to leach from the soil (N pool) to the groundwater. The leaching rate *LEA* (kg ha^{-1}

263 day^{-1}) is defined as a first order process as:

$$LEA = f \cdot SIN / \Delta t \tag{6}$$

$$f = (1 - exp^{-a\frac{wal}{\theta d}}) \tag{7}$$

$$wal = q \cdot \Delta t \tag{8}$$

267 where *f* is a factor, ranging between [0, 1], to determine the portion of SIN that leaches into groundwater during a time

268 step Δt. *a* is unit-less leaching factor. θ is the soil porosity. *d* is the soil depth. *wal* [L] is the water available for

269 leaching during Δt. *wal* can be estimated using the Darcy fluxes *q* [LT^{-1}], which are provided by the flow simulations

270 for each cell of the mesh. Physically, *f* is a function of the ratio between *wal* and the volume of soil voids $\theta \cdot d$,

271 representing the ability of water to flush the SIN. This formulation of *LEA* is modified from the ones used in *Pierce*

272 *et al.*, [1991], *Shaffer et al.* [1991] and *Wijayantiati et al.* [2017], to comply with the spatially-distributed

273 HydroGeoSphere model.

274 **Table 2**. The parameters for the N pool and nitrate transport. The parameters with a range are calibrated. The
275 adjustable ranges are selected to cover the values that the parameters can potentially take on or the values reported
276 by the referred literature.

Parameter	Description	Range	Reference	Best-fit value
N pool				
d	Soil depth	Fixed	*Yang et al.* [2018]	0.5 m
N Input	N external input	Fixed	*Nguyen et al.* [2021]	180 kg ha^{-1} yr^{-1}
h	protection coefficient	Fixed	*Van Meter et al.* [2017]	0.3 [-]
k_a	Mineralization coef. (DON$_a$)	[0 - 0.7]	*Yang et al.* [2021]	0.011 day^{-1}
k_p	Mineralization coef. (DON$_p$)	[0 - 0.7]	*Yang et al.* [2021]	0.0008 day^{-1}
λ_s	Denitrification coef. (soil)	[0 - 0.7]	*Yang et al.* [2021]	0.0007 day^{-1}
$p1$	Parameter for plants-uptake	[60 - 160]	*Van Meter et al.* [2017]	160 kg ha^{-1}
$p2$	Parameter for plants-uptake	[0 - 10]		9.8 kg ha^{-1}
$p3$	Parameter for plants-uptake	[1 - 60]		25.6 day
$p4$	Parameter for plants-uptake	Fixed		63 day
a	Leaching factor	[0 – 100]		0.154 [-]
Transport				
λ	Denitrification coef. (water)	[0 - 0.7]	*Yang et al.* [2021]	0.0072 day^{-1}
a_L	Longitudinal dispersity	Fixed		8 m
a_T	Transverse dispersivity	Fixed		0.8 m

277

278 The N pool is positioned on the top part of the aquifer, used as a boundary condition for the DIN (nitrate) transport.
279 Advective-dispersive transport of DIN in the flow system is simulated using HydroGeoSphere (Figure 2b).
280 Degradation (denitrification in groundwater) during transport is considered as a first order process. Degradation is not
281 considered on the land surface (denitrification in surface flow), where aerobic conditions likely deactivate
282 denitrification and residence time is short. To implement the evapoconcentration effect in the transport model, ET is
283 assumed to remove DIN mass without altering the DIN concentration of the water, and to inject that mass back to the
284 SIN pool. This represents a precipitation process from DIN to SIN, which is the inverse process of leaching (Figure
285 2b). There are two reasons for doing that: (i) the physical process of ET causing the immobilization of DIN can be
286 mathematically considered, and (ii) the N mass balance can be conserved as the plants-uptake is already considered
287 in the N pool according to the plant growth function (Equation 4 and 5), being independent from the ET flux.

288 Regarding the parameters, the soil depth, within which the N pool is implemented, is set to 0.5 m. N external input is
289 180 kg ha^{-1} yr^{-1} according to Nguyen et al. (2021), where the nitrate balance was simulated for the larger upper Selke
290 catchment that contained our studied catchment. The external N input is assumed to be spatiotemporally constant due
291 to the limited information on its variation in space and time. The protection coefficient h is fixed as 0.3 according to
292 the values reported in *Van Meter et al.* [2017]. The sowing date $p4$ is fixed as 63 days according to the fact that sowing

293   activities and plant growth start in early March. Longitudinal and transverse dispersivity values were 8 m and 0.8 m,

294   respectively. Other parameters were set to be adjustable and calibrated (Table 2).
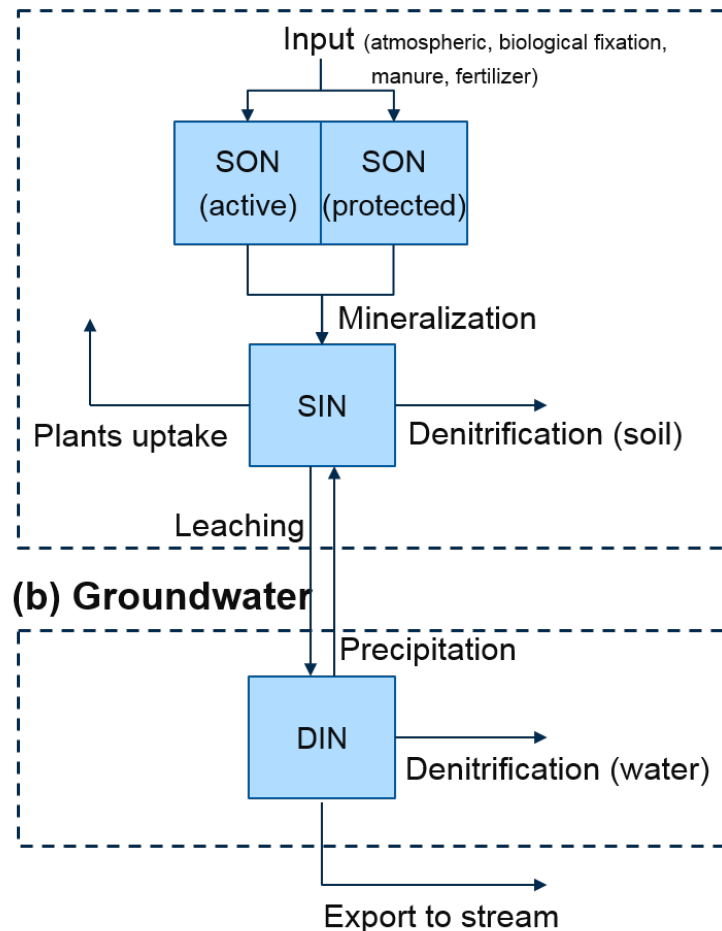
295

296   **Figure 2.** Conceptual framework for nitrogen (N) fluxes (a) in the soil (N pool), and (b) after leaching into the

297   groundwater.

298

299

300   *Transport calibration*

301   As the flow parameters (e.g., hydraulic conductivity and porosity) were already calibrated in *Yang et al.* [2018] using

302   data sets of discharge and groundwater levels. In this study, the calibration was only performed for the transport t̶To

303   get reasonable parameter values for the N pool and N transport, a calibration was performed for the transport. The

304   software package PEST [*Doherty and Hunt,* 2010] was used. PEST uses the Marquardt method [*Marquardt, 1963*] to

305   minimize a target function by varying the values of a given set of parameters until the optimization criterion is reached.

306   We used the measured C_Q and N surplus as the ~~data sets~~target variables for comparison with the simulated ones.~~.~~ The

307   N surplus, which is the annual amount of N remaining in the soil after consumption by plant-uptake, was estimated as

308   48.8 kg ha^{-1} yr^{-1} [*(Yang et al.,* 2021)]. As two different data sets (C_Q and N Surplus) were used, a weighting scheme
309   was used such that the defined multi-objective function was not dominated by one data set.

310   Note that the entire model calibration (for flow and transport) actually followed a procedure of two steps: first for
311   flow, and second for transport. Alternatively, the flow and transport parameters can be calibrated at one step by
312   defining the multi-objective function using all the data sets (discharge, groundwater levels, C_Q and N surplus). The
313   potential effect of the two different calibration procedures on the modeling results should be further explored, however,
314   being out of the main focus of this study. We consider the two-step calibration procedure to be acceptable, because
315   our result showed that it was sufficient to reach an acceptable model performance for both flow and transport
316   (described later).

317   Several transport parameters were fixed at the values selected according to prior information, such that the degree of
318   freedom in the calibration can be reduced as much as possible (Table 2). In total eight parameters were adjustable and
319   calibrated (Table 2), because they were the key parameters to determine the N fluxes in soil and groundwater. Their
320   adjustable ranges were selected according to the literature or to cover the values that the parameters can potentially
321   realistically reach (Table 2). The calibration was carried out for the period from Jul 1999 to Jul 2003, during which
322   the data sets are available. First, the flow and transport were simulated in the catchment of the base scenario (original
323   topography, section 2.1), for the period from Jul 1999 to Jul 2003. Secondly, PEST was used to obtain a best fit
324   between the simulated results and the data sets by varying the parameter values. We used the measured C_Q and N
325   surplus as the data sets. The N surplus, which is the annual amount of N remaining in the soil after consumption by
326   plant uptake, was estimated as 48.8 kg ha^{-1} yr^{-1} (Yang et al., 2021). Note that the simulation period from Jul 1999 to
327   Jul 2003 was only used for model calibration, rather than for the actual simulations with the eleven catchments of
328   different topographic slope. After calibration, the model with the best-fit parameter values can well replicate the
329   measured C_Q with a Nash-Sutcliffe efficiency (NSE) of 0.75 (see Figure S1 in the supporting information). The
330   simulated N surplus was 50.7 kg ha^{-1} yr^{-1}, comparable to the measured value.

331   The best-fit parameter values from the base scenario were also used for the all other scenarios with catchments of
332   different topographic slope, assuming that the parameters do not change with the change of topographic slope. In total,
333   we simulated the flow and nitrate transport for eleven scenarios (11 catchments of different topographic slope). For
334   each scenario, the simulations were run for 100 years with identical boundary conditions for each year. The first 99
335   years were used as a spin-up phase to assure a dynamic equilibrium (i.e. to achieve simulated variables, such as heads
336   and concentrations, that are identical between years), and the last year was used for actual observation and analysis.
337   The CPU time of each simulation was ~4 hours.

3.2 Water ages

339   The water stored in a catchment (storage), Q and ET can all be characterized by age distributions, for they comprise
340   water parcels of different age from precipitation events that occurred in the past. The age distributions need to be
341   calculated for each aforementioned scenario to assess the responses of water ages on catchment topographic slope.

342   Our model setup (with virtual catchments and identical climate for each year) allowed us to perform long-term

343   numerical tracer experiments and to extract the age distributions.

344   We assumed that inert tracers of uniform concentration existed in precipitation. The tracers were applied to the land

345   surface as a third-type (Cauchy) boundary condition and were subjected to transport modeling. Tracer can exit the

346   aquifer via the outfluxes Q and ET. We considered a period of 200 years for the tracer experiments, which was

347   sufficiently long to ensure convergence of the computed water ages. The 200 years period was partitioned into 2400

348   months (Δt = 1 month). A different tracer was used for each of the periods resulting in a total of 2400 distinct tracers.

349   The injection of tracer i started with the precipitation at the beginning of its associated period t_0^i and lasted throughout

350   the period. The advective-dispersive multi-solute transport was simulated using HydroGeoSphere. The first 199 years

351   of the simulation period were used as a spin-up phase to ensure a dynamic equilibrium of the calculated ages,

352   minimizing the influence of the initial conditions. The last year was used for the actual observations and the

353   computation of age distributions. Solving the transport of the 2400 tracers would be computationally expensive.

354   However, because the climate (flow boundary conditions) was identical for each year, the transport simulation was

355   performed only for the first 12 tracers that covered the course of a year. Based on these results, the results for the other

356   2388 tracers were manually reproduced (e.g., by shifting the concentration breakthrough curves of the 12 tracers in

357   time while maintaining the shapes).

358   For each tracer, the breakthrough curves of the mass-fluxes of Q and ET, as well as the mass in storage were reported.

359   For a specific time t, the age distributions for Q/ET/storage were computed by calculating the mass fraction of each

360   tracer using:

361
$$p_{Q/ET/S}(T,t) = \frac{M^i(t)}{\Delta t \sum M^i(t)} \tag{9}$$

362

363   where $p_Q(T,t)$, $p_{ET}(T,t)$ are the age distributions of Q, ET (equivalent to backward transit time distributions - TTDs),

364   and $p_S(T,t)$ is the age distributions of water in storage (equivalent to the residence time distribution - RTD). $M^i(t)$ is

365   the mass-flux of the tracer i in Q or ET, or the mass stored in catchment at time t, $\sum M^i(t)$ is the sum of $M^i(t)$ over

366   all tracers. T is the age ranging within $[t - t_0^i - \Delta t, t - t_0^i]$ for tracer i.

367   For each scenario, the CPU time of the tracer experiment was ~8 hours. Based on the age distributions, we calculated

368   the mean discharge age $T_Q(t)$, which is equivalent to the mean discharge transit time (simply referred to as 'discharge

369   age' in the following sections). We calculated the young water fraction in streamflow $YF_Q(t)$, which is the fraction of

370   streamflow with an age younger than three months (also referred to as 'young streamflow fraction' [*Jasechko et al.*

371   2016]). Similarly, the ET age $T_{ET}(t)$ and the young water fraction in ET $YF_{ET}(t)$ can be calculated as well (more

372   details are described in Text S1 of the supporting information). Their responses to changes in topographic slope were

373   analyzed.

374

4 Results and discussion

4.1 Dynamics of water ages and nitrogen fluxes

Driven by the seasonality of the climate, the simulated Q, the young water fractions YF, and the water ages all show seasonal fluctuations. Figure 3 shows these fluctuations for the base scenario (original topography). Q reaches its maximum towards the end of the wet winter in late February and reaches its minimum during the drier late summer in mid-September. Total Q consists of a portion of groundwater discharge (including the flow via vadose zone) and a portion generated via surface-runoff during events of high precipitation (Figure 3a). The calculated YF_{ET} is smallest in April and largest in November (Figure 3b), while YF_Q is smallest in August and largest in February. ET generally has larger young water fractions than Q as ET has a higher probability to remove young water from the shallow soil rather than the older water from the deeper aquifer. Especially during the dry season (summer), most precipitation can

385 be quickly removed by ET. The water ages of Q and ET show generally opposite fluctuation patterns for *YF* (Figure

386 3c). The ET age ranges from 70 to 115 days, being younger than Q that has the age ranging from 109 to 180 days.

387
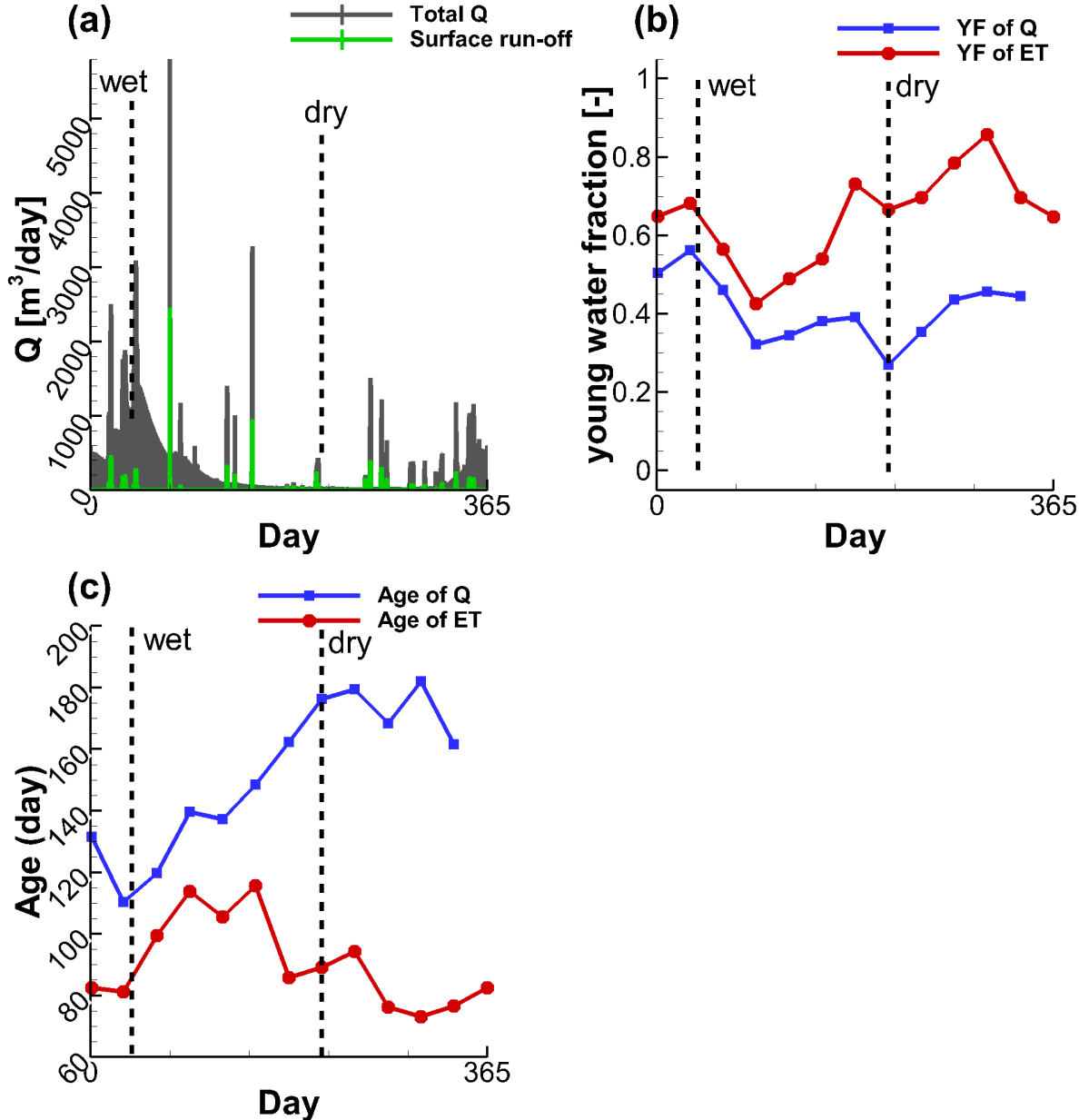
Figure 3. Simulated (**a**) Q, (**b**) young water fractions in streamflow (YF_Q) and evapotranspiration (YF_{ET}), and (**c**) water

389 ages for the catchment of the base scenario. The *YF* and water ages are monthly averages.

390

391 The simulated C_Q shows strong seasonality with maxima in the wet and minima in the dry period, fitting the measured

392 C_Q data well (Figure 4a). Figure 4b lists the calculated annual N mass balance in the catchment of the base scenario.

393 The organic (SONa + SONp) and inorganic (SIN) N load in the soil are 470 kg ha^{-1} and 43 kg ha^{-1}, respectively. The

394 SON accounts for 92% of the total N load, which is consistent with the study of Stevenson [1995] where the organic

395   N fraction was reported to be greater than 90%. The mineralization converts SON into SIN with a rate of 180 kg ha^{-1}

396   yr^{-1}. This rate is equal to the external N input because this way a steady-state of the annual N mass balance was reached

397   in the simulations. About 76% of the input N flux is taken up by the vegetation (136 kg ha^{-1} yr^{-1}). 20% is consumed

398   by denitrification (36 kg ha^{-1} yr^{-1}), either in the soil (before leaching) or in the groundwater (after leaching). The

399   remaining 4% reaches the stream water and is exported out of the catchment (6 kg ha^{-1} yr^{-1}). The simulated

400   mineralization flux is within the range of [14–187] kg ha^{-1} yr^{-1} reported by *Heumann et al.* [2011] for their study sites

401   in central Germany. The simulated plant uptake and leaching fluxes are comparable to the values suggested in Nguyen

402   et al. [2021] for the same area (120 kg ha^{-1} yr^{-1} for plant uptake and [15–60] kg ha^{-1} yr^{-1} for leaching). The simulated

403   denitrification rate is within the range [8–51] kg ha^{-1} yr^{-1} reported in Hofstra and Bouwman [2005] for 336 agricultural

404   soils located worldwide. Moreover, 80% and 20% of the leaching N are consumed by denitrification during transport

405   in the groundwater and exported to stream water, respectively. These portions are generally comparable to those

406   reported in Nguyen et al. [2021] (61% and 39%, respectively). Therefore, the simulated N loads and fluxes for the

407   catchment of the base scenario are considered to be acceptable.

408   Figure 4c shows the temporal variation of the N load and fluxes. It demonstrates that low levels of SIN are maintained

409   by high plant-uptake before the dry summer arrives (May – June), such that there is little SIN available for leaching.

410   The SIN load reaches its minimum when plant uptake reaches its maximum (marker a in Figure 4c). The cessation of

411   plant-uptake during the dry period leads to the increase of the SIN load as well as the increase of the leaching rate.

412   The mineralization in winter is significantly reduced due to the dropping temperatures, cutting the SIN supply. This

413   results in the SIN load reaching its high peak in the middle of November (marker b in Figure 4c) and subsequent

414   decrease due to increased leaching and eventually plant uptake. These seasonal fluctuation patterns are generally

415   consistent with the knowledge of N fluxes reported in previous studies [Dupas et al., 2017; Nguyen et al., 2021]. For

416   DIN load in water, it reaches its maximum generally when the leaching weakens in the beginning of March (marker c

417   in Figure 4c), and reaches the minimum just before the leaching process becomes active again in the end of August

418   (marker d in Figure 4c). These low and high peaks of SIN and DIN loads can also be identified by their spatial

419   distributions in the catchment (see Figure S2 in the supporting information).

420   Seasonal variations of C_Q can be directly influenced either by the fluctuation of the nitrate leaching into groundwater,

421   or by fluctuations in the degradation in groundwater associated with varying transit times (quantified by the young

422   water fraction in streamflow YF_Q). These two influences represent the effect from the variability in N source and in N

423   transport, respectively. Linear regression analysis shows that C_Q is correlated with leaching flux rate and YF_Q with

424   Spearman rank-correlation coefficients of 0.1 and 0.34, respectively (Figure 5). The seasonal fluctuations of C_Q and

425   leaching flux are temporally out of phase. The maximum leaching occurs in December, while the maximum C_Q is

426   reached two months later in February (Figure 5a). The minimum leaching occurs in April, while the minimum C_Q is

427   reached around September. This behavior indicates that C_Q responds later to the changes in N leaching, which is

428   reasonable because the leaching nitrate needs time to travel from the shallow soil to streamflow. The fluctuation of

429   C_Q and YF_Q are more synchronized, proven by the fact that both maxima are reached in February (wet, Figure 5b) and

430   minima occur generally in the dry summer time. Field observations in mountainous central German catchments also

431   indicate that C_Q varies seasonally, with maxima during the wet winter and minima during the dry summer [Dupas et

432   al., 2017]. These seasonal fluctuations of C_Q and YF_Q were frequently explained using the "inverse storage effect"

433   [*Harman*, 2015; *Yang et al.* 2018]: during the wet season Q has a strong preference for young water associated with

434   higher concentrations, which would not occur during dry periods due to the deactivation of the shallow fast flow

435   processes. These patterns generally suggest that the C_Q fluctuation is more attributed to the variability in the N

436   transport rather than to the variability in the N source, echoing previous observations that 80% of the leaching N mass

437   is degraded during transport. However, it is still hard to tell whether the N source or the N transport is dominating the

438   C_Q fluctuation.

439

440
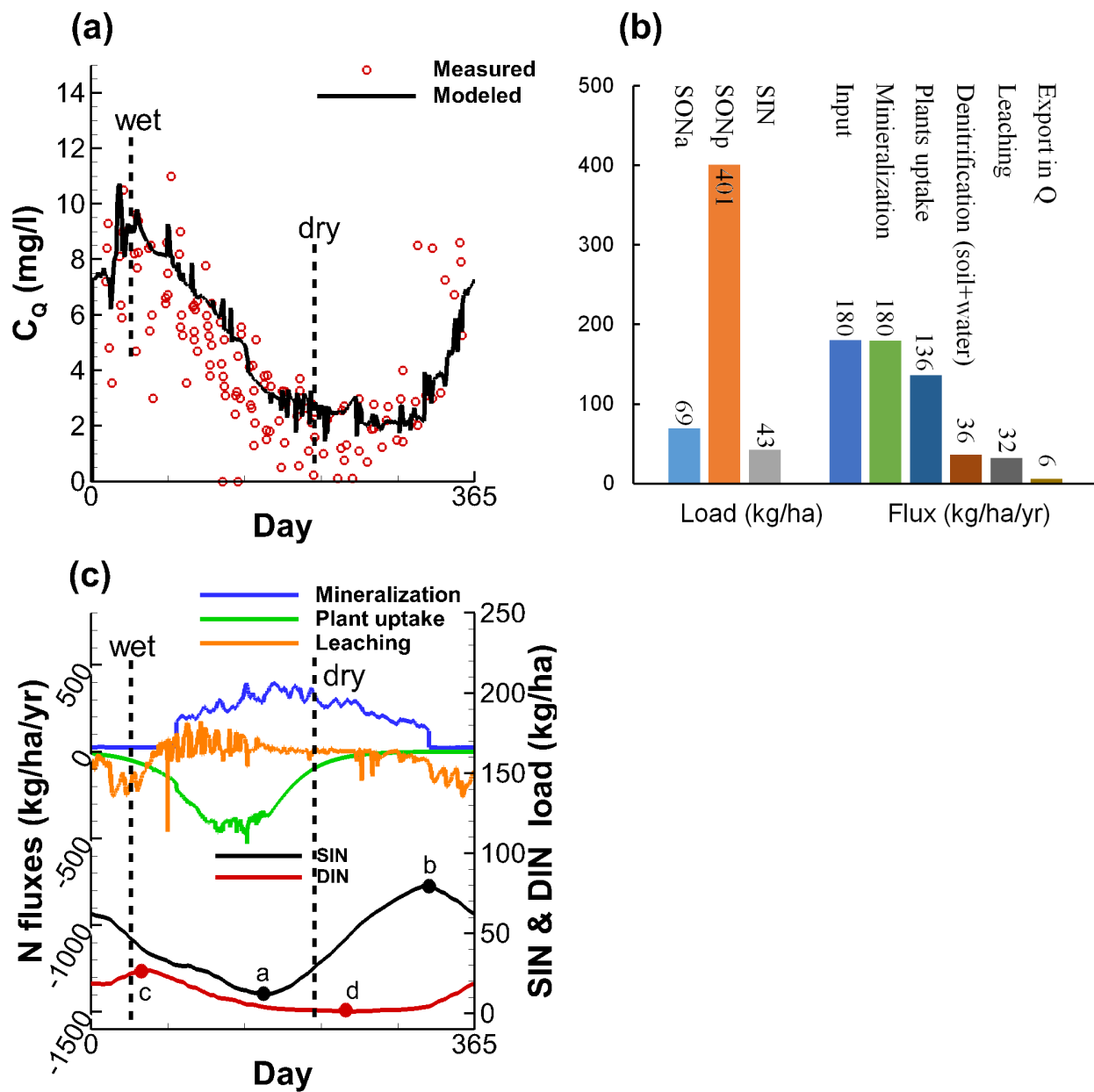
Figure 4. Simulated (**a**) In-stream nitrate concentration C_Q, (**b**) N loads and fluxes, and (**c**) time-variable N fluxes for the catchment of the base scenario. Note that the measured C_Q in (a) includes all the measurements from 2001 to 2010.

441
442
443
444
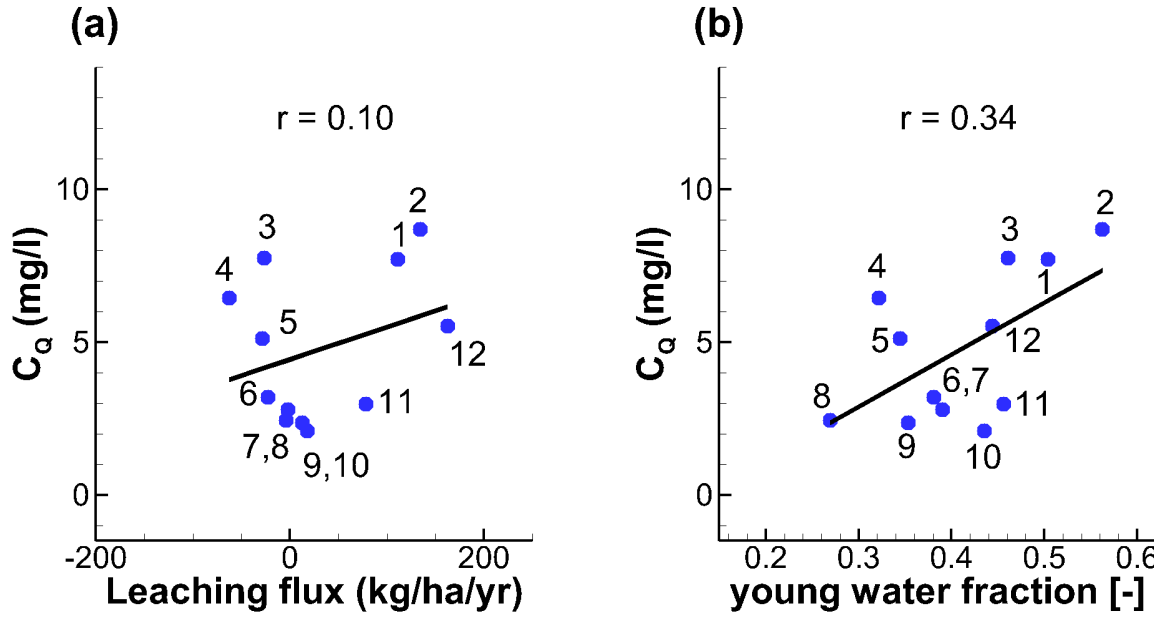
Figure 5. Comparing the monthly averaged C_Q with (**a**) the leaching flux and (**b**) the young water fractions of Q. The black lines are linear fits of the two variables, with r being the Spearman rank-correlation coefficient. The numbers refer to the months.

4.2 Effect of topographic slope on flow

With the help of our simulations, it is possible to systematically explore the influence of topographic slope on the water flow and N fluxes. Figure 6 shows the responses of temporally-averaged Q and ET, the groundwater table depth, and flow weighted mean YF_Q and YF_{ET} to the changes of topographic slope. Under a constant climate, the changes of topographic slope can reshape the water flow via influencing flow partitioning between Q and ET. More water is taken up by ET and less water becomes Q in flatter landscapes (Figure 6a). These patterns can be explained by the change of groundwater table depth (Figure 6b), as shallower groundwater tables can be reached by the vegetation in flatter landscapes where ET therefore has a higher chance to remove water from the subsurface. The simulated YF_Q and YF_{ET} show generally increasing and decreasing patterns, respectively, when the topographic slope decreases (Figure 6c), demonstrating that young streamflow is more prevalent in flatter landscape and young ET is more prevalent in steeper landscapes. However, the increasing pattern of YF_Q does not continue in steep catchments with slopes > 1:60. Topographic slope changes YF_Q not only in terms of its mean value, but also in terms of its temporal variation. Figure 6d indicates that the maximum and minimum YF_Q are reached in February and August for the steepest catchment (slope 1:20), respectively, and in November and April for the flattest catchment (slope 1:1000).
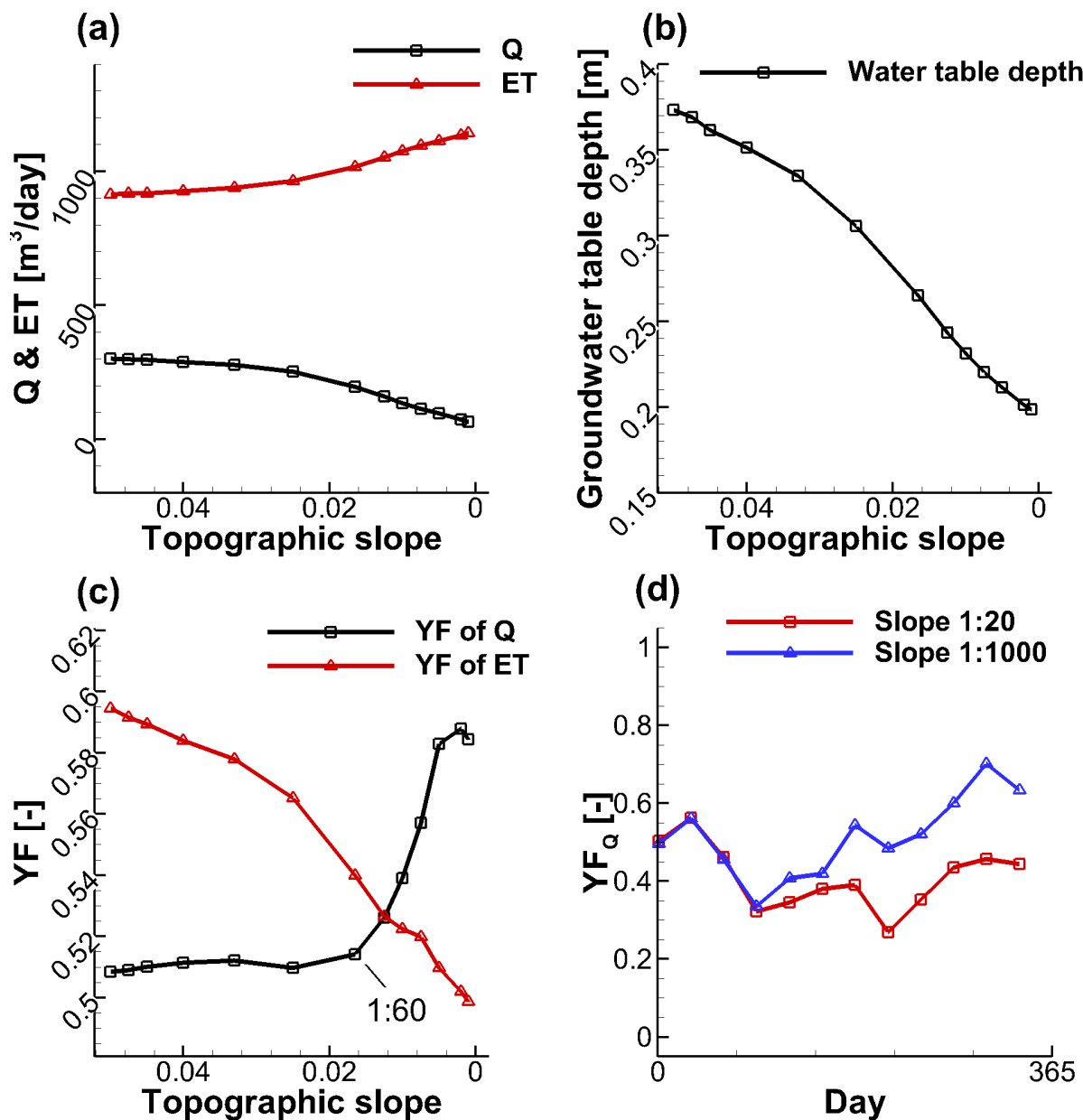
Figure 6.- The simulated (**a**) Q and ET, (**b**) spatially-averaged depth of the groundwater table from the land surface, (**c**) young water fraction in streamflow YF_Q and evapotranspiration YF_{ET}, in relation to the topographic slope for the simulated catchments. (**d**) temporal variations of YF_Q for a steep landscape (slope 1:20) and a flat land scape (slope 1:1000).

Interpreting the response of the YF_Q to topographic slope mechanistically requires a closer look at the flow processes using a cross-sectional view. We plotted the subsurface flow fields for the wet season at a cross-section of the catchments with slopes 1:20 and 1:1000 (Figure 7).

474   Figure 7a reveals that the hillslope part of the catchment with a slope of 1:20 is largely unsaturated so that the flow

475   paths in this area are characterized by vertical infiltration. In contrast, the valley bottom is fully saturated. Overall,

476   34% of the subsurface domain is characterized by vertical flow (flow in 34% of the total aquifer volume is more

477   vertical than horizontal). For this scenario two main discharge routes to the stream can be identified: (i) A fraction of

478   the groundwater flows through the fully saturated zone and exits the aquifer to the stream, and (ii) another fraction

479   exits the aquifer via seepage near to where the groundwater table intersects the land surface, indicated by a large

480   exchange flux (from subsurface to surface, positive). The seepage represents a preferential flow path allowing for

481   discharge via overland flow instead of discharge via the sub-surface with longer transit times. Note that both of the

482   discharge routes provide the pathways for the rainfall falling on the top hillslope to reach the stream.

483   When the slope is reduced to 1:1000, the flow pattern experiences significant changes (Figure 7b) compared to the

484   catchment with a slope of 1:20. Several hydrologic studies have described two different flow systems in aquifers: (i)

485   a recharge-limited system where the thickness of the unsaturated zone is sufficient to accommodate any water-table

486   rise and thus the elevation of the groundwater table is limited by the recharge, and (ii) a topography-limited system

487   where the groundwater table is close or connected to the land surface such that any fluctuation in groundwater table

488   can result in considerable change in surface runoff [*Werner and Simmons*, 2009; *Michael et al.,* 2013]. In the selected

489   cross sections, the steeper one (slope 1:20) is a partially topography-limited system (Figure 7a) (the hillslope is

490   recharge-limited while the valley bottom is topography-limited). The flat one (slope 1:1000) is transformed into a

491   fully recharge-limited system (from Figure 7b) due to the reduced hydraulic head gradients. This transformation leads

492   to three main effects: (i) The seepage flow vanishes because the groundwater table disconnects from the land surface.

493   The seepage route that would discharge water from the top of hillslope to the stream is cut off, (ii) the infiltration

494   processes is weakened, indicated by the fact that the portion of subsurface domain characterized by vertical flow is

495   reduced from 34% to 18%, and (iii) local flow cells are more likely to form, where water infiltrates to the aquifer and

496   eventually exits the aquifer via ET rather than via flow to the stream (Figure 7b, the local flow cells are more

497   pronounced in the dry season, see Figure S3-b in the supporting information).

498   Because of the three aforementioned effects, the connectivity between the stream and the more distant hillslopes is

499   significantly reduced. Precipitation falling farther from the stream has a lower chance to reach the stream and a higher

500   change to be intercepted by ET on its way to the stream. The hillslope that used to generate old streamflow does not

501   contribute to streamflow anymore. While precipitation water close to the stream has a higher chance to contribute to

502   streamflow. We concluded that the increase of the YF_Q in flat landscapes is due to this reduction of the longer flow

503   paths and the persistence of shorter flow paths, as indicated by the computed TTDs (Figure 7c).

504
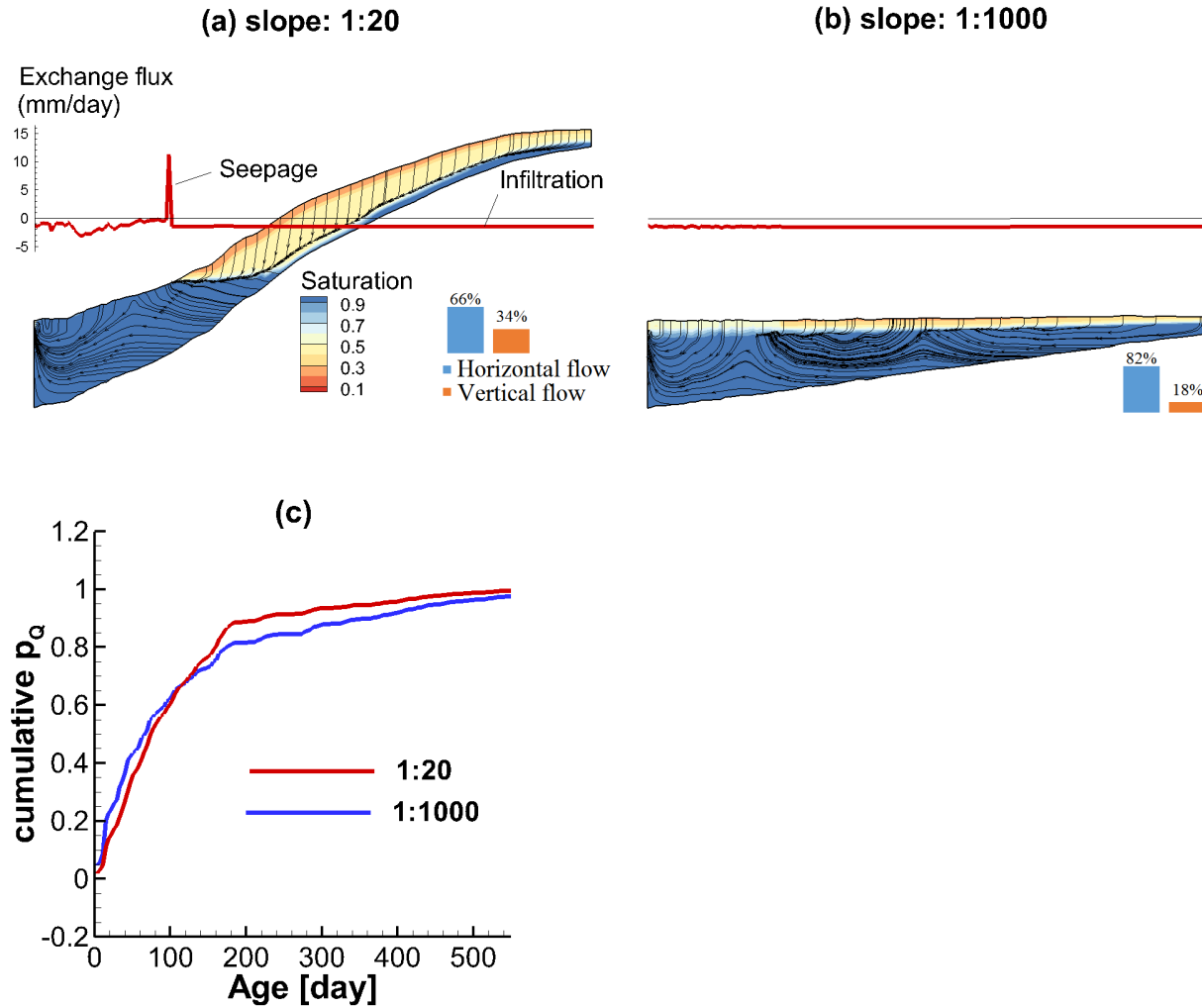
Figure 7. Cross-sectional view of saturation, flow paths, and exchange fluxes between the surface and the subsurface in the wet season (February) for catchments with topographic slope (**a**) 1:20, and (**b**) 1:1000. The cross-section is marked in Figure 1a. The black lines represent the flow paths. The red curves show exchange fluxes (along the cross-sectional profiles), positive values indicate seepage to the land surface and negative values indicate infiltration to the subsurface. (**c**) The computed cumulative TTDs for Q during the wet season (February), for the catchment with topographic slope of 1:20 and 1:1000.

In summary, we identified a generally increasing pattern of YF_Q in response to the decreasing topographic slope. When the landscape becomes flatter, the hydraulic head gradient as the main driving force changes the aquifer from a partially topography-limited system to a recharge-limited system that is more likely to form local flow cells.

4.3 Effect of topographic slope on N export

Simulated results show that the topographic slope can influence the N loads and fluxes in catchments. Figure 8a demonstrates that SIN tends to be higher in flatter and lower in steeper landscapes. This generally indicates that a flat

520   landscape has a higher potential to retain N in the soil. However, the DIN is not significantly influenced by the

521   topographic slope. N fluxes of leaching and export to the stream exhibit the opposite pattern. For the N fluxes, the

522   leaching into groundwater decreases with the decrease of topographic slope (Figure 8b). This is mainly because the

523   flow velocity (influencing the leaching rate according to equation 6) in flatter landscape is lower due to the reduced

524   hydraulic head gradient. Comparing the time-variable leaching between the steepest and flattest catchments (slope

525   1:20 and 1:1000, Figure 8c), it can be observed that the leaching reduction in the flatter landscape mainly occurs in

526   the wetting period (Nov to Dec). This may be because the response of flow velocity in the flatter catchment is not as

527   large as that in the steeper catchment when the system transitions from dry to wet conditions. A large portion of the

528   leached N mass has been degraded during transport in the groundwater, with the fraction rising from 80% in the

529   steepest landscape to 95% in the flattest landscape (Figure 8b). Mechanically, the reduced connectivity between the

530   stream and more distant hillslopes in flatter landscapes inhibits the N export to the stream promoting the degradation

531   by increasing the N residence time in the catchment. Subsequently, the N export shows a decreasing pattern with the

532   decrease of topographic slope (Figure 8b).

533   The calculated flow-weighted mean C_Q shows a decreasing trend in response to the decreasing topographic slope

534   (Figure 8d), from 7.3 mg l^{-1} in the steepest catchment to 4.2 mg l^{-1} in the flattest catchment. Even though both Q and

535   N export show decreasing patterns with the decrease of topographic slope, the N export decreases to a higher degree

536   than Q, indicated by the normalized values (Figure 8e). Comparing the time-variable C_Q between the steepest and

537   flattest catchments (slope 1:20 and 1:1000, Figure 8f), it can be observed that the topographic slope influences the C_Q

538   in two ways: (i) The C_Q is generally lower (but not always) in the flatter landscape over most of the time in a year, and

539   (ii) the high peaks of C_Q in flatter landscapes are delayed in time. However, the high concentrations always occur in

540   the wet periods (Jan – Apr) and low concentrations always occur in the dry periods (Jul – Oct).

541
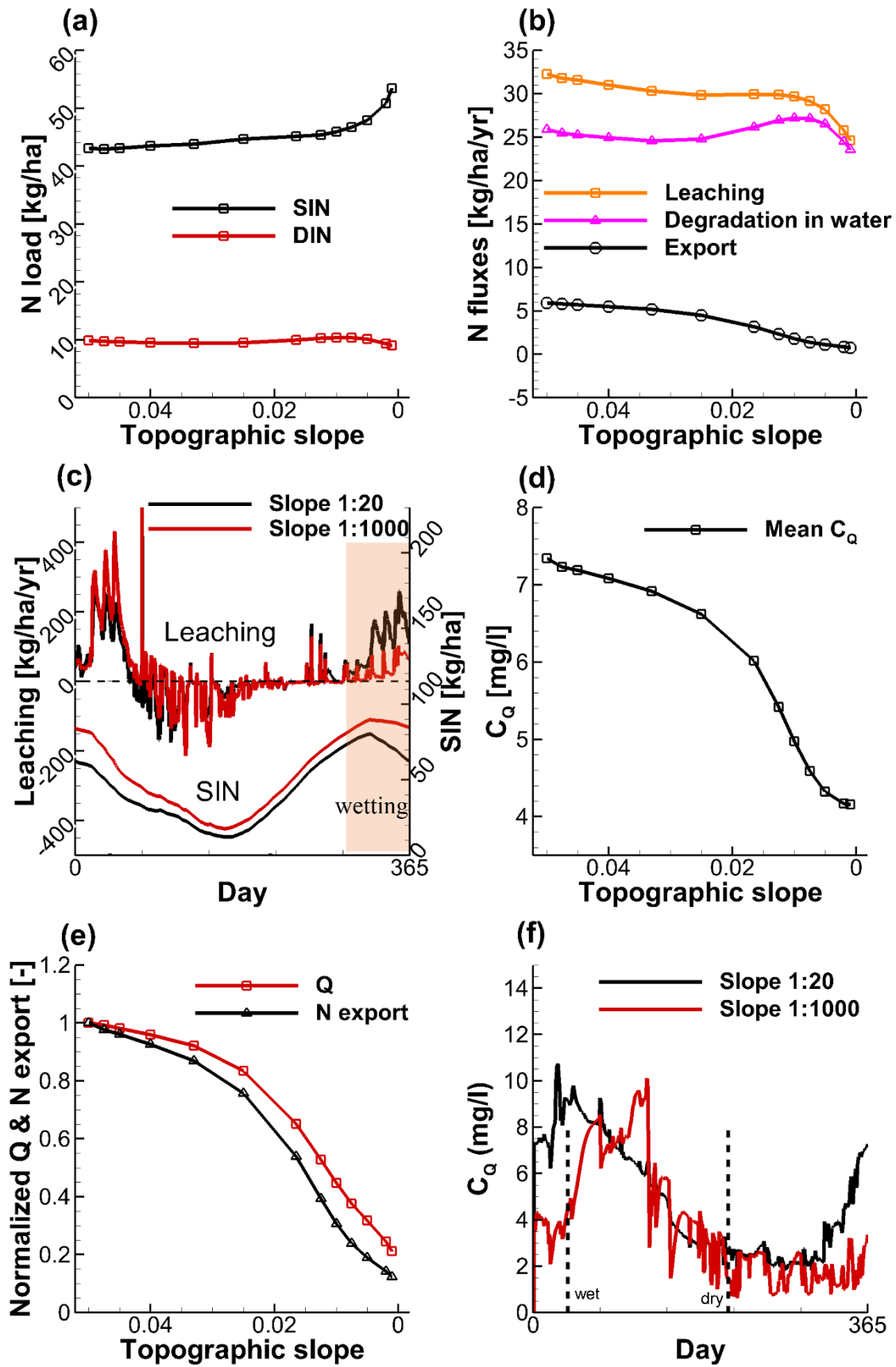
Figure 8.- The simulated (**a**) N loads, (b) N fluxes in relation to the topographic slope for the simulated catchments. (**c**) Comparison of the time variable N loads and fluxes between a steep (slope 1:20) and a flat land scape (slope 1:1000). The simulated (d) flow-weighted mean C_Q, and (e) the normalized Q and N export (normalized to their values of the base scenario) in relation to the topographic slope. (**f**) Comparison of the time variable C_Q between a steep (slope 1:20) and a flat land scape (slope 1:1000). Note that for the leaching fluxes in (**c**), positive values are referred to as the N leaching from the soil to the groundwater, negative values are referred to as the precipitation of N from groundwater to the soil by the evapoconcentration effect. The vertical dashed lines indicate the time when the catchment reaches the wettest (left) and the driest (right) conditions.

4.4 Discussion

Jasechko et al., [2016] reported that (the logarithm of) catchment topographic slope was significantly negatively correlated with young streamflow fractions with a spearman rank correlation of -0.36. This conclusion was made statistically based on their observed 254 sites. Our numerical study based on the eleven catchments with different slopes but identical climate conditions resulted in more physically-based information that goes beyond such statistical correlations. Our results confirm that young streamflow fraction and slope generally exhibit a negative correlation. Additionally, our results show that the young water fraction in ET is positively correlated with the slope.

From the steepest landscape to the flattest landscape, catchments are likely to transition from a partially topography-limited flow system to a recharged limited system, due to the reduction of hydraulic gradient. The groundwater table is closer to the land surface when the landscape becomes flatter. The larger young streamflow fraction in flatter landscapes is consistent with the statement made by *Jasechko et al*. [2016] that the young streamflow fraction is more prevalent in flatter catchments which are characterized by more shallow lateral flow and less vertical infiltration. This phenomenon is also consistent with a negative correlation between groundwater table depth and young streamflow fraction, which has been frequently reported [*Bishop et al., 2004; Seibert et al., 2009; Frei et al., 2010; Jasechko et al., 2016*]. Using the insight into the flow processes of the catchment, we found that the connectivity between the stream and the more distant hillslopes is reduced in flatter landscape, due to the reduced seepage flow, the weakened infiltration and the formation of local flow cells that do not deliver flow to the stream. Our study points out that the reduction of this connectivity, which results in the reduction of the longer flow paths and the persistence of shorter flow paths, causes the increase of the young streamflow fraction.

Basically, the position of the groundwater table, flow path lengths and flow velocities, which are all different for different topographic slopes, jointly affect the young streamflow fractions. Besides that, temporal variability of these three factors drives the distinct responses of the young streamflow fraction to topographic slope between seasons. In our simulated catchments, the negative correlation between young streamflow fraction and topographic slope is more pronounced in the flat landscapes with slopes < 1:60. This demonstrates that the system is complex and apparently contains various threshold effects disturbing a straightforward monotonous relationship between catchment characteristics (e.g. slope) and young water fraction (or streamflow concentration). In this sense, systematically

578 investigating the reaction of the flow dynamics to catchment characteristic is necessary, rather than assuming a
579 straightforward cause-effect relationship that can be misleading.

580 Our results demonstrate that stream water quality is potentially less vulnerable in flatter landscapes. The flatter
581 landscapes tend to retain more N mass in the soil and export less N mass to the stream. This behavior can be attributed
582 to (i) the reduced leaching in flat landscapes since the decreased flow velocity physically reduces the potential of water
583 to solve and transport the solute, and (ii) the increased potential of degradation because the connectivity between the
584 stream and hillslope is blocked (i.e. there is more time for decay). Our results also show that higher C_Q is more
585 prevalent in steeper landscapes. Note that this is concluded for average concentrations. Observations from the Selke
586 catchment, central Germany show that the C_Q is not always lower in flatter regions [*Dupas et al.*, 2017; Nguyen *et al.*,
587 2022]. In the future more attention should be paid to the temporal variation and the time-scale concerning the effect
588 of topographic slope on C_Q. Additionally, our results show that we can expect lower C_Q and higher young streamflow
589 fractions in flatter landscapes. This suggests that, with regard to the N transport in catchments, a large young
590 streamflow fraction is not sufficient for high levels of C_Q. This phenomenon has not yet been reported to the best of
591 our knowledge.

592 Concerning the seasonal variations of C_Q, our results showed that significant seasonal variation can be expected under
593 temperate humid climates regardless of topographic slope. The high peak concentrations occurred in the wet and the
594 low in the dry seasons, being consistent with the findings of previous studies [*Benettin et al.* 2015; *Harman*, 2015;
595 *Kim et al.*, 2016; *Yang et al.*, 2018]. However, the topographic slope can slightly shift the high peak concentrations in
596 time.

597

598 **4.5 Limitations and outlook**

599 The cross-comparison between catchments with differing topographic slopes provides physically-based insights into
600 the effects of topographic slope on nitrate export responses in terms of N fluxes and mean concentrations. However,
601 this study is limited in scope in that it neglects other factors that may also have important impacts on the young
602 streamflow and nitrate export processes:

603 First, our study only considered the aquifers that is unconfined with an impermeable base and prescribed heterogeneity.
604 Other catchment characteristics such as landscape aspect, catchment area, aquifer permeability or drainage ability,
605 aquifer depth, stream bed elevation, fractured bedrock permeability, bedrock slope and shape of basin can potentially
606 change the flow patterns and age composition in streamflow [*McGlynn et al.,* 2003*; Broxton et al.,* 2009; *Sayama and*
607 *McDonnell*, 2009; *Stewart et al.*, 2010; *Jasechko et al.*, 2016; *Heidbüchel et al.*, 2013, 2020; *Zarlenga and Fiori*,
608 2020]. For example, aquifers with high permeability or highly fractured bed rock are more likely to use deep rather
609 than shallow flow paths and preferential discharge routes that lead to rapid drainage. Apart from that, it was reported
610 that hydrological features such as precipitation variability, ET, antecedent soil moisture are also significantly linked
611 to transit times [*Sprenger* et al., 2016; *Wilusz et al.* 2017; *Evaristo et al.*, 2019; *Heidbüchel et al.*, 2013, 2020]. For
612 example, compared to uniform precipitation, event-scale precipitation is more likely to trigger rapid surface runoff

613   and intermediate flow, such that the contribution of young water from storage to streamflow can be increased.

614   Therefore, further research should consider a more complex model structure involving various heterogeneity and

615   climate types.

616   Second, several main simplifications were used in the formulation of the nitrate transport processes. (i) Transport

617   modelling employed a constant degradation rate coefficient assuming that transit time was the only factor to determine

618   degradation. This assumption neglected other factors that can spatially and temporally affect denitrification rates, such

619   as temperature, redox boundaries (e.g., high oxygen concentration in shallow flow paths), the amount of other nutrients

620   (e.g. carbon), which also contribute to the seasonality in nitrate concentrations [*Böhlke et al.*, 2007]. Apart from that,

621   we did not account for the long-term (decades [*Van Meter et al.*, 2017]) nitrate legacy effect as the dissolved nitrate

622   in groundwater reservoirs degraded continuously in our model, which would not occur in older reservoirs where the

623   denitrification is very slow or deactivated (e.g. due to the lack of a carbon source). (ii) The N external input source

624   was uniformly applied across the land surface in our modelling. However, strong source heterogeneity may exist in

625   catchments. For example, the N external input varies between land uses or along the soil profile [*Zhi et al.*, 2019].

626   This spatial source heterogeneity could affect the seasonal variations of C_Q [*Musolff et al.*, 2017; *Zhi et al.*, 2019] and

627   should be considered in further research.

628   While the numerical model provided general insights, there was potential uncertainty in the simulated results. Firstly,

629   the aforementioned simplifications may introduce model structural errors. Secondly, the model calibration was only

630   constrained by limited data sets, which may lead to the non-uniqueness in the model parameters. Both of the aspects

631   may introduce uncertainty in the simulated N loads and fluxes. Future work should be devoted to better constrain the

632   model parameters, either by enhancing the concentration data quality through more frequent measurements or by

633   providing additional data sets related to the N pool.

634   Despite these limitations, the numerical experiments in this study could clearly identify the response of young

635   streamflow and nitrate export to topographic slope under a humid seasonal climate, and show that hydraulic gradient

636   is an important factor causing flow field differences between the catchments. This was achieved by using the

637   advantages of a physically-based flow simulation that allows for a more mechanistic evaluation of flow processes,

638   which would be impossible with a purely data driven analysis based on, e.g., isotopic tracers only.

639

640   **5 Conclusions**

641   Previous data driven studies suggested that catchment topographic slope impacts the age composition of streamflow

642   and consequently the in-stream concentrations of certain solutes [*Jasechko et al.*, 2016]. We attempted to find more

643   mechanistic explanations for these effects. We chose the small agricultural catchment 'Schäfertal' in Central Germany

644   and, based on it, generated eleven synthetic catchments of varying topographic slope. The groundwater and overland

645   flow, and the N transport in these catchments were simulated using a coupled surface-subsurface model. Water age

646   compositions for Q and ET were determined using numerical tracer experiments. Based on the calculated flow patterns,

647   young water fractions in streamflow YF_Q, N mass fluxes and in-stream nitrate concentration C_Q, we systematically

648 assessed the effects of varying catchment topographic slopes on the nitrate export dynamics in terms of the mass fluxes
649 and annual mean concentration levels. The main conclusions of this study are:

650   ● Under the considered humid climate, YF_Q is generally negatively correlated to topographic slope. When the
651   landscape becomes flatter, the hydraulic head gradient is the main driving force to change the aquifer from a
652   partially topography-limited system to a recharge-limited system, reducing the connectivity between the
653   stream and the more distant hillslopes. This change results in the reduction of longer flow paths and the
654   persistence of shorter flow paths, subsequently causing the flatter landscapes to generate younger streamflow.

655   ● The flatter landscapes tend to retain more N mass in soil and export less N mass to the stream. These patterns
656   are attributed to (i) the reduced leaching in flat landscape as the decreased flow velocity physically reduces
657   the potential of water to transport the solute towards the stream, and (ii) the increased potential of degradation
658   as the connectivity between the stream and hillslope is blocked and the solute stays inside the aquifer longer.

659   ● For the considered catchment, the annual mean C_Q shows a decreasing trend in response to the decreasing
660   topographic slope, because the N export decreases to a higher degree than Q. Flatter landscapes tend to
661   generate larger young streamflow fractions (but lower C_Q), suggesting that a large young streamflow fraction
662   is not sufficient for a high level of C_Q.

663 Overall, this study provided a mechanistic perspective on how catchment topographic slope affects young streamflow
664 fraction and nitrate export patterns. The use of a fully-coupled flow and transport model extended the approach to
665 investigate the effects of catchment characteristics beyond the frequently used tracer data-driven analysis. It can be
666 used for similar studies of other catchment characteristics and for other solutes. The results of this study improved the
667 understanding of the effects of certain catchment characteristics on nitrate export dynamics with potential implications
668 for the management of stream water quality and agricultural activity, in particular for catchments in temperate humid
669 climate with pronounced seasonality. Given the limitations of this study, future work should be devoted to improve
670 the degradation formulation, to investigate further catchment characteristics, as well as to consider various climate
671 types.

672

673

674 **Notation**

675 t [T] time
676 T [T] age / transit time / residence time
677 J [LT^{-1}] precipitation
678 ET [LT^{-1}] evapotranspiration
679 Q [LT^{-1}] discharge / streamflow
680 p_S [-] age distribution of storage
681 $p_{ET/Q}$ [-] age distribution for evapotranspiration / discharge, equivalent to TTD
682 C [ML^{-3}] concentration

683   C_Q $[\mathrm{ML^{-3}}]$ in-stream solute (nitrate) concentration

684   T_Q $[\mathrm{ML^{-3}}]$ age (transit time) of discharge

685   YF_Q [-] young water fraction in streamflow, or young streamflow fraction

686   YF_{ET} [-] young water fraction in ET

687   SON $[\mathrm{M\,L^{-2}}]$ soil organic nitrogen

688   SIN $[\mathrm{M\,L^{-2}}]$ soil inorganic nitrogen

689   DIN $[\mathrm{M\,L^{-2}}]$ dissolved inorganic nitrogen in water

690

691

692

Code/Data availability

694 All data used in this study are listed in the supporting information and uploaded separately to HydroShare [Yang,
695 2022].

696

Author contributions

698 JY: conceptualization, methodology, software, formal analysis, visualization, writing - review & editing; QW:
699 modelling, analysis, writing; IH: writing - review & editing; CL: conceptualization, methodology, review & editing;
700 YX: methodology; AM: conceptualization; JF: conceptualization, review & editing.

701

Competing interests

703 The authors declare that they have no conflict of interest.
704

Acknowledgments

706 This research was supported by the National Key Research and Development Project (JY & CL: 2021YFC3200500),
707 the National Natural Science Foundation of China (JY: No. 52009032, CL: 51879088), and the Fundamental Research
708 Funds for the Central Universities (JY: No. B210202019), and the Natural Science Foundation of Jiangsu Province
709 (CL: BK20190023). We thank the editorial board for handling our manuscript, especially Prof. Dr. Insa Neuweiler
710 and two anonymous reviewers, whose constructive comments helped improve the manuscript.

711

712

References

714 Anis, M. R., & Rode, M. (2015). Effect of climate change on overland flow generation: A case study in central
715 Germany. Hydrological Processes, 29(11), 2478–2490.

716   Benettin, P., Y. van der Velde, S. E. A. T. M. van der Zee, A. Rinaldo, and G. Botter (2013), Chloride circulation in
717   a lowland catchment and the formulation of transport by travel time distributions, Water Resources Research, 49(8),
718   4619–4632, doi: 10.1002/wrcr.20309.

719   Benettin, P., J. W. Kirchner, A. Rinaldo, and G. Botter (2015), Modeling chloride transport using travel time
720   distributions at plynlimon, wales, Water Resources Research, 51(5), 3259–3276, doi:10.1002/2014WR016600.

721   Bishop, K., Seibert, J., Köhler, S. and Laudon, H. (2004), Resolving the Double Paradox of rapidly mobilized old
722   water with highly variable responses in runoff chemistry. Hydrol. Process., 18: 185-189.
723   https://doi.org/10.1002/hyp.5209.

724   Botter, G., Bertuzzo, E., & Rinaldo, A. (2010). Transport in the hydrologic response: Travel time distributions, soil
725   moisture dynamics, & the old water paradox. Water Resources Research, 46(3).
726   https://doi.org/10.1029/2009WR008371.

727   Botter, G., Bertuzzo, E., & Rinaldo, A. (2011). Catchment residence and travel time distributions: The master equation.
728   Geophysical Research Letters, 38(11). https://doi.org/10.1029/2011GL047666.

729   Böhlke, J. K., M. E O'Connell, and K. L Prestegaard (2007), Ground water stratification and delivery of nitrate to an
730   incised stream under varying flow conditions, Journal of environmental quality, 36, 664–80,
731   doi:10.2134/jeq2006.0084.

732   Broxton, P. D., P. A. Troch, and S. W. Lyon (2009), On the role of aspect to quantify water transit times in small
733   mountainous catchments, Water Resour. Res., 45, W08427, doi:10.1029/2008WR007438.

734   Doherty, J., Hunt, R., 2010. Approaches to highly parameterized inversion – a guide to using PEST for groundwater-
735   model calibration. Technical Report, USGS Survey Scientifi Investigations Report. 2010-5169.

736   Dupas, R., A. Musolff, J. W. Jawitz, P. S. C. Rao, C. G. Jäger, J. H. Fleckenstein, M. Rode, and D. Borchardt (2017),
737   Carbon and nutrient export regimes from headwater catchments to downstream reaches, Biogeosciences, 14(18),
738   4391–4407, doi:10.5194/bg- 14-4391-2017.

739   Evaristo, J., Kim, M., van Haren, J., Pangle, L. A., Harman, C. J., Troch, P. A., & McDonnell, J. J. (2019).
740   Characterizing the fluxes and age distribution of soil water, plant water, and deep percolation in a model tropical
741   ecosystem. Water Resources Research, 55(4), 3307-3327.

742   Frei, S., Lischeid, G. and Fleckenstein J.H. (2010) Effects of micro-topography on surface-subsurface exchange and
743   runoff generation in a virtual riparian wetland – a modeling study, Advances in Water Resources, 33(11):1388-1401.

744   Haag, D., Kaupenjohann, M., 2001. Landscape fate of nitrate fluxes and emissions in central Europe: a critical review
745   of concepts, data, and models for transport and retention. Agric. Ecosyst. Environ. 86 (1), 1–21.

746   Harman, C. J. (2015), Time-variable transit time distributions and transport: Theory and application to storage-
747   dependent transport of chloride in a watershed, Water Resources Research, 51(1), 1–30, doi:10.1002/2014WR015707.

748   Harman, C. J. (2019). Age-Ranked Storage-Discharge Relations: A Unified Description of Spatially Lumped Flow
749   and Water Age in Hydrologic Systems. Water Resources Research, 55(8), 7143-7165.

750   Heidbüchel, I., P. A. Troch, and S. W. Lyon (2013). Separating physical and meteorological controls of variable transit
751   times in zero-order catchments. Water Resources Research, 49, 7644–7657, doi:10.1002/2012WR013149.

Heidbüchel, I., J. Yang, A. Musolff, P. Troch, T. Ferré, J. H. Fleckenstein (2020). On the shape of forward transit time distributions in low-order catchments. Hydrology and Earth System Sciences, doi: 10.5194/hess-2019-440.

Hrachowitz, M., O. Fovet, L. Ruiz, and H. H. G. Savenije (2015), Transit time distributions, legacy contamination and variability in biogeochemical 1/fΊś scaling: how are hydrological response dynamics linked to water quality at the catchment scale?, Hydrological Processes, 29(25), 5241–5256, doi:10.1002/hyp.10546.

Heumann, S., Ringe, H., B̈ottcherBöttcher, J., 2011. Field-specific simulations of net N mineralization based on digitally available soil and weather data. I. Temperature and soil water dependency of the rate coefficients. Nutr. Cycl. Agroecosyst. 91 (2), 219–234. https://doi.org/10.1007/s10705-011-9457-x.

Hofstra, N., Bouwman, A.F., 2005. Denitrification in agricultural soils: summarizing published data and estimating global annual rates. Nutr. Cycl. Agroecosyst. 72 (3), 267–278. https://doi.org/10.1007/s10705-005-3109-y.

Hrachowitz, M., P. Benettin, B. M. Van Breukelen, O. Fovet, N. J. Howden, L. Ruiz, Y. Van Der Velde, and A. J. Wade (2016), Transit times-the link between hydrology and water quality at the catchment scale, Wiley Interdisciplinary Reviews: Water, 3(5), 629–657.

Jasechko, S., Kirchner, J., Welker, J. et al. Substantial proportion of global streamflow less than three months old. Nature Geosci 9, 126–129 (2016). https://doi.org/10.1038/ngeo2636

Kaandorp, V. P., Louw, P. G. B., Velde, Y., & Broers, H. P. (2018). Transient Groundwater Travel Time Distributions and Age‐Ranked Storage‐Discharge Relationships of Three Lowland Catchments. Water Resources Research, 54, 4519– 4536. https://doi.org/10.1029/2017WR022461

Kim, M., L. A. Pangle, C. Cardoso, M. Lora, T. H. Volkmann, Y. Wang, C. J. Harman, and P. A. Troch (2016), Transit time distributions and storage selection functions in a sloping soil lysimeter with time-varying flow paths: Direct observation of internal and external transport variability, Water Resources Research, 52(9), 7105–7129.

Knoll, L., Breuer, L., & Bach, M. (2020). Nation-wide estimation of groundwater redox conditions and nitrate concentrations through machine learning. Environmental Research Letters, 15, 064004. https://doi.org/10.1088/1748-9326/ab7d5.

Kolbe, T., de Dreuzy, J. R., Abbott, B. W., Aquilina, L., Babey, T., Green, C. T., et al. (2019). Stratification of reactivity determines nitrate removal in groundwater. Proceedings of the National Academy of Sciences, 116(7), 2494–2499. https://doi.org/10.1073/pnas.1816892116.

Li, Y., Chen, Y., Li, Z., 2019. Dry/wet pattern changes in global dryland areas over the past six decades. Glob. Planet. Chang. 178, 184–192. https://doi.org/10.1016/j. gloplacha.2019.04.017.

Lindström, G., C.P. Pers, R. Rosberg, J. Strömqvist, and B. Arheimer (2010): Development and test of the HYPE (Hydrological Predictions for the Environment) model – A water quality model for different spatial scales, Hydrol. Res., 41.3–4, 295–319, 2010.

Marquardt, D.W., 1963. An algorithm for least-squares estimation of nonlinear parameters. J. Soc. Ind. Appl. Math. 11 (2), 431–441.

McGlynn, B., J. McDonnell, M. Stewart, and J. Seibert (2003), On the relationships between catchment scale and streamwater mean residence time, Hydrol. Processes, 17, 175– 181, doi:10.1002/hyp.5085.

788   Michael, H.A., Russoniello, C.J., Byron, L.A., 2013. Global assessment of vulnerability to sea-level rise in
789   topography-limited and recharge-limited coastal groundwater systems. Water Resour. Res. 49, 1–13.

790   Musolff, A., C. Schmidt, B. Selle, and J. H. Fleckenstein (2015), Catchment controls on solute export, Advances in
791   Water Resources, 86, 133–146.

792   Musolff, A., J. H. Fleckenstein, P. S. C. Rao, and J. W. Jawitz (2017), Emergent archetype patterns of coupled
793   hydrologic and biogeochemical responses in catchments, Geophysical Research Letters, 44(9), 4143–4151,
794   doi:10.1002/2017GL072630.

795   Nguyen, T. V., Kumar, R., Lutz, S. R., Musolff, A., Yang, J., & Fleckenstein, J. H. (2021). Modeling nitrate export
796   from a mesoscale catchment using storage selection functions. Water Resources Research, 57, e2020WR028490.
797   https://doi.org/10.1029/2020WR028490

798   Nguyen, T. V., Kumar, R., Musolff, A., Lutz, S. R., Sarrazin, F., Attinger, S., & Fleckenstein, J. H. (2022). Disparate
799   seasonal nitrate export from nested heterogeneous subcatchments revealed with StorAge Selection functions. Water
800   Resources Research, 58, e2021WR030797. https://doi.org/10.1029/2021WR030797

801   Oldham, C. E., D. E. Farrow, and S. Peiffer (2013), A generalized damköhler number for classifying material
802   processing in hydrological systems, Hydrology and Earth System Sciences, 17(3), 1133–1148, doi:10.5194/hess-17-
803   1133-2013.

804   Pierce, F. J., Shaffer, M. J., Halvorson, A. D. 1991. Chapter 12: Screening procedure for estimating potentially
805   leachable nitrate-nitrogen below the root zone. Managing Nitrogen for groundwater Quality and Farm Profitability,
806   Soil Science Society of America, USA. pp.259-283

807   Rinaldo, A., P. Benettin, C. J. Harman, M. Hrachowitz, K. J. McGuire, Y. Van Der Velde, E. Bertuzzo, and G. Botter
808   (2015), Storage selection functions: A coherent framework for quantifying how catchments store and release water
809   and solutes, Water Resources Research, 51(6), 4840–4847.

810   Rivett, M. O., Buss, S. R., Morgan, P., Smith, J. W. N., & Bemment, C. D. (2008). Nitrate attenuation in groundwater:
811   A review of biogeochemical controlling processes. Water Research, 42(16), 4215–4232.
812   https://doi.org/10.1016/j.watres.2008.07.020

813   Rodriguez, N. B., McGuire, K. J., & Klaus, J. (2018), Time-varying storage-water age relationships in a catchment
814   with a mediterranean climate. Water Resources Research, 54(6), 3988-4008.

815   Sayama, T. & McDonnell, J. J. (2009), A new time-space accounting scheme to predict stream water residence time
816   and hydrograph source components at the watershed scale. Wat. Resour. Res. 45, W07401.

817   Seibert, J., Grabs, T., Köhler, S., Laudon, H., Winterdahl, M., and Bishop, K.: Linking soil- and stream-water
818   chemistry based on a Riparian Flow-Concentration Integration Model, Hydrol. Earth Syst. Sci., 13, 2287–2297,
819   https://doi.org/10.5194/hess-13-2287-2009, 2009.

820   Sprenger, M., Seeger, S., Blume, T., & Weiler, M. (2016), Travel times in the vadose zone: Variability in space and
821   time. Water Resources Research, 52, 5727-5754.

822   Therrien, R., McLaren, Sudicky, R. E., & Panday, S. (2010). Hydrogeosphere: A three-dimensional numerical model
823   describing fully-integrated subsurface and surface flow and solute transport, Groundwater Simulations Group.
824   Waterloo, ON: University of Waterloo.

825   Shaffer, M. J., Halvorson, A. D., Pierce, F. J. 1991. Chapter 13: Nitrate leaching and economic analysis package

826   NLEAP: model description and application. Managing Nitrogen for groundwater Quality and Farm Profitability, Soil

827   Science Society of America, USA. pp.285-322

828   Smith, R. L., Böhlke, J. K., Garabedian, S. P., Revesz, K. M., & Yoshinari, T. (2004). Assessing denitrification in

829   groundwater using natural gradient tracer tests with 15N: In situ measurement of a sequential multistep reaction. Water

830   Resources Research, 40, W07101. https:// doi.org/10.1029/2003WR002919.

831   Stewart, M. K., Morgenstern, U. & McDonnell, J. J. (2010), Truncation of stream residence time: how the use of stable

832   isotopes has skewed our concept of streamwater age and origin. Hydrol. Process. 24, 1646-1659.

833   van der Velde, Y., G. De Rooij, J. Rozemeijer, F. Van Geer, and H. Broers (2010), Nitrate response of a lowland

834   catchment: On the relation between stream concentration and travel time distribution dynamics, Water Resources

835   Research, 46(11).

836   Stevenson, F.J., 1995. Humus chemistry: genesis, composition, reactions, Second Edition, Wiley. J Chem Educ. doi:

837   10.1021/ed072pA93.6, ISBN: 978-0-471-59474-1, 512 pp.

838   van der Velde, Y., P. J. J. F. Torfs, S. E. A. T. M. van der Zee, and R. Uijlenhoet (2012), Quantifying catchment-scale

839   mixing and its effect on time-varying travel time distributions, Water Resources Research, 48(6), n/a–n/a,

840   doi:10.1029/2011WR011310, w06536.

841   Van Meter, K. J., N. B. Basu, and P. Van Cappellen (2017), Two centuries of nitrogen dynamics: Legacy sources and

842   sinks in the mississippi and susquehanna river basins, Global Biogeochemical Cycles, 31(1), 2–23,

843   doi:10.1002/2016GB005498.

844   Werner, A. D., and C. T. Simmons (2009), Impact of sea-level rise on seawater intrusion in coastal aquifers, Ground

845   Water, 47, 197-204.

846   Wilusz, D. C., Harman, C. J., & Ball, W. P. (2017). Sensitivity of catchment transit times to rainfall variability under

847   present and future climates. Water Resources Research, 53(12), 10231-10256.

848   Wijayantiati, Y., Budihardjo, K., Sakamoto Y., Setyandito, O. (2017). Topsoil N-budget model in orchard farming to

849   evaluate groundwater nitrate contamination. IOP Conf. Series: Earth and Environmental Science 109 (2017) 012034.

850   doi:10.1088/1755-1315/109/1/012034.

851   Yang, J., I. Heidbüchel, A. Musolff, F. Reinstorf, and J. H. Fleckenstein (2018), Exploring the dynamics of transit

852   times and subsurface mixing in a small agricultural catchment, Water Resources Research, 54(3), 2317–2335,

853   doi:10.1002/2017WR021896.

854   Yang, J., Heidbüchel, I., Musolff, A., Xie, Y., Lu, C.*, Fleckenstein, J.H. (2021). Using nitrate as a tracer to constrain

855   age selection preferences in catchments with strong seasonality, Journal of Hydrology, 603, 126889. doi:

856   https://doi.org/10.1016/j.jhydrol.2021.126889.

857   Yang, J. (2022). DS2022-1YJ, HydroShare,

858   http://www.hydroshare.org/resource/e266298e55834617a26242f6af9687e1

859   Yang, X., Jomaa, S., & Rode, M. (2019). Sensitivity analysis of fully distributed parameterization reveals insights

860   into heterogeneous catchment responses for water quality modelling. Water Resources Research, 55, 10935–10953.

861   https://doi.org/10.1029/2019WR025575.

862 Yang, X., Jomaa, S., Zink, M., Fleckenstein, J. H., Borchardt, D., & Rode, M. (2018). A new fully distributed model

863 of nitrate transport and removal at catchment scale. Water Resources Research, 54, 5856–5877.

864 https://doi.org/10.1029/2017WR022380.

865 Zarlenga, A., & Fiori, A. (2020). Physically based modelling of water age at the hillslope scale: The Boussinesq age

866 equations. HYDROLOGICAL PROCESSES, 34(12), 2694-2706.

867 Zarlenga, A., Fiori, A., & Cvetkovic, V. (2022). On the interplay between hillslope and drainage network flow

868 dynamics in the catchment travel time distribution. HYDROLOGICAL PROCESSES, 36(3) [10.1002/hyp.14530].

869 Zhi, W., L. Li, W. Dong, W. Brown, J. Kaye, C. Steefel, and K. H. Williams (2019), Distinct source water chemistry

870 shapes   contrasting   concentration-discharge   patterns,   Water   Resources   Research,   55(5),   4233–4251,

871 doi:10.1029/2018WR024257.